nature portfolio

Peer Review File

Integration of high strength, flexibility, and room-temperature plasticity in ceramic nanofibers

Corresponding Author: Professor Bin Ding

Parts of this Peer Review File have been redacted as indicated to remove third-party material.

This file contains all reviewer reports in order by version, followed by all author rebuttals in order by version.

Version 0:

Reviewer comments:

Reviewer #1

(Remarks to the Author)
In this article, the authors have demonstrated that single ceramic nanofibers (CNFs) exhibit a good combination of high strength, superior deformability, and room temperature plasticity. This achievement is attributed to the optimized crystalline-amorphous dual-phase (DP) structure in CNFs, which includes reduced fiber defects and nanograin aggregation and increased crystalline-amorphous interfaces. The improved mechanical performance, opens up potential applications for CNFs in extreme scenarios such as mechanical shocks, high-frequency vibrations, and repeated twisting. The manuscript needs substantial revising and proper referencing. In addition, the supplementary figures are not discussed and poorly organized which can be improved for better understanding of the content. Hence, I would recommend the journal to publish this manuscript once the authors successfully revised the manuscript and addressed the following revisions/comments.

Major Comments:

1. Could the authors please explain their rationale behind selecting 1 fs as the timestep size and address any possible missing interactions or inaccuracies due to this choice? The size of the timestep in molecular dynamics simulations should, typically, be an order of magnitude smaller than the fastest motion time scale in the system. For TiO2 modeled as flexible molecules with flexible bonds, the system has translational, vibrational, rotational, and torsional degrees of freedom (DOFs). Among these, the vibrational DOF is the fastest, with a typical time scale of ~1 fs. At high temperatures, such as 3300 K, this motion becomes even more significant due to the elevated kinetic energy of the atoms. Therefore, to capture high-accuracy interactions, an optimal timestep should be less than 1 fs, unless otherwise specific reasons are mentioned. Is there a convergence test? Or is this to minimize round-off errors? For reference, a previous study (J. Phys. Chem. C 2007, 111, 19, 6920–6926) used a 0.5 fs timestep for simulating TiO2.

2. MD simulation methodology section (Section 2.1: Conceptual design) is not comprehensively written and lacks proper referencing. For example, in pg. 5, “By employing the Large-scale Atomic/Molecular Massively Parallel Simulator (LAMMPS) and the Matsui-Akaogi force field, we obtained amorphous and DP TiO2 models (Fig. 1c and 1d).” Here, references to LAMMPS code and the force field are missing. Additionally, how the following line—“Then, the tensile simulations were performed on box models (147455 atoms) with a strain rate of 109 s−1 along the x-axis (Fig. 1f and 1g)33, 34”—is related to the cited Refs. 33 and 34.

3. Did the authors quantify the nanocrystals within the amorphous matrix? A measure of a quantification, say volume fraction of nanocrystals, in Model-2 and Model-3 can help comprehend the role of such nanocrystals in enhancing strength and ductility. Is it possible that from Model-1 to Model-3, the improvement can be explained with the Rule of Mixtures? If not, then can other effective medium theories (EMTs)–Maxwell (can be thought as Model-3) or Rayleigh (Model-2)–be utilized to explain the observed results?

4. The manuscript, especially the ‘structural analysis’ section (Section 2.3), lacks coherency and purpose of the analyses conducted. Here are some examples,

a. Pg. 11: “Their diameters were aligned to exclude size-dependent interference (Supplementary Fig. 13).” Here,

supplementary Fig. 13 does not contain any quantitative information on diameters.
b. Pg. 11: “Additionally, calculations based on the Langmuir theory verify the same tendency.” Here, the tendency is not discussed clearly and the statement is vague. Also, no citation to Langmuir theory for readers is provided for completeness.
c. Pg. 11: “… and micropores in Model-1 may serve as the weakest link to CNF fracture (Fig. 3d). Sintering is a crucial …” Here, sentences and transitions lack coherency and consistency.
d. How the supplementary Fig. 15 explains the weight loss of Model-1 is not discussed. The text: “In addition, a counterintuitive rising- plunging trend observed between 438.84-509.11 °C may result from deep residual carbon oxidation and consequent gas release.” What is the purpose of this sentence and supplementary Fig. 15c?

5. In Figure 1g, could the authors include strain values in addition to the number of steps? It appears that Model-2 and Model-3 undergo crack/void nucleation after 18.2x104 and 47x104 steps, respectively. This indicates that Model-2 and Model-3 experience cracks at applied strain values of 18.2% and 47%, respectively, given that timestep size = 1 fs, strain rate = 10-9 s-1, and strain applied at every step (dynamic stretching). Could the authors please clarify how these simulation strain values can be compared with experimentally-obtained strain values (e.g., σ¬u and σ¬f)?

6. Did the authors compare the stress-strain curves obtained from push-to-pull (PTP) experimental setup with those obtained from MD simulations? Figure 4c presents the experimentally-extracted stress-strain response, but it is unclear as to how well or poorly the MD-computed stress-strain response curve agrees with the former ones.

7. The authors claim that dangling bonds enhance feasibility: “The presence of numerous oxygen vacancies in Model-3 suggests the presence of dangling bonds, thus chemically supporting the feasibility (Fig. 4i)62.” Here, can the authors define ‘feasibility’ and clarify how the presence of dangling bonds enhance such feasibility? If it is about the bond switching phenomenon, then did the authors observe any bond switching in this case?

8. In Model-3, is it the nanocrystal regions that help with the ductility or the amorphous matrix? The text: “Importantly, the amorphous matrix gains improved structural continuity and an increased internal interface, acting as a soft boundary to efficiently transfer and dissipate stress. These multiple deformation mechanisms encourage the fracture of CNFs to occur after plastic deformation. Eventually, as shown in Fig. 1g, Model-3 may fracture due to localized stress concentration in shear bands within the amorphous regions, rather than initiating in the nanocrystal domains26, 35, 36, 37.” Model-1 and Model-3 both contain shear bands in the amorphous matrix and the only difference is that in Model-3, there are nanocrystals that can act as hindrance to shear bands. So, it seems like that the presence of nanocrystals help with the ductility and strength. Can the authors clarify?

Minor Comments:

1. In Fig.1b, it looks like the red arrows at the cracks, grain boundaries, and shear bands denote dislocation pile-ups. Could the authors use some other way to visualize such deformation mechanisms?

2. The font size in Fig. 4i is too small. Can the authors use larger font size and an equal picture size for all other figures, including the supplementary ones. For example, supplementary Fig. 12 is not properly sized, compared to Fig. 12.

3. The authors demonstrate that nucleation regulation enhances strength and deformability. In Model-3, random nucleation points result in nanograins emerging further apart, preventing aggregation. However, how does the algorithm prevent interleaving where grains grow and coalesce together? Could the authors provide more details on this aspect?

4. The difference in the SAED patterns between Model-2 and Model-3, as shown in the insets of Fig. 3e, is not clearly visualized. Also, please state the purpose/significance of such patterns.

5. It is very interesting that controlled nucleation can result in a CNF with superior mechanical properties. While this finding can significantly improve the understanding of CNF’s material response, it is worth exploring how a patterned nucleation scheme, as used in J. Appl. Phys. 134, 154301 (2023) and Appl. Phys. Lett. 122, 133101 (2023), where patterned nanodiamond regions are reported to be a better stress dissipator and conductor than random nucleation points, can influence the mechanical properties of Model-3?

Reviewer #2

(Remarks to the Author)
I co-reviewed this manuscript with one of the reviewers who provided the listed reports. This is part of the Nature Communications initiative to facilitate training in peer review and to provide appropriate recognition for Early Career Researchers who co-review manuscripts.

Reviewer #3

(Remarks to the Author)
The present manuscript by Qiang et al. reports on the synthesis and thorough structural and mechanical characterisation of three distinct model TiO2 ceramic nanofibers in the ~300nm range. The authors show as stepwise improvement of mechanical characteristics of the individual fibres by (I) removal of multi-scale defects (model1 > model2) and (II) de-

clustering of the nanocrystalline TiO2 grains within the amorphous matrix (model2>model3). This structural optimization has been initially studied using MD simulations to guide the synthesis route. The authors have presented a ligand exchanged linear-particle sol, which was able to be electrospun without any polymer templates, reducing the formation of larger defects to a minimum. Furthermore, the addition of small percentages of spherical-particle sol was used to achieve well separated nucleation spots for nanocrystals, reducing the formation of stress-concentrating grain boundaries. The resulting improvement in mechanical response was investigated using state-of-the art nanomechnical testing for single fibres (PTP-tension) experiments as well as a creative, albeit not very accurate, way of estimating flexibility (in-situ fibre bending).
The authors have presented their train-of-thought and execution in an easy-to-follow and intuitive manner. The experimental investigations seem sound and the combination of different methods for structural (SEM, TEM, XRD) as well as energetic/chemical (DSC,DMA,XPS) investigations spark confidence in their conclusions. The work has been conducted on a well-studied model material system, but the results should be applicable for a wide variety of ceramics, potentially leading to novel designs in various 2D (fibre mats) or 3D (aeorgels) applications.
A few minor questions that should be addressed:

1. While I understand that the chosen mechanical in-situ investigations are not trivial to perform, having only one experiment per material state does not spark a lot of confidence in the reproducibility of the results. Have the authors conducted multiple experiments? If so it would be beneficial to show the results at least as supplementary material to give the reader an idea about the uncertainties in yield onset and ductility values. The same is true for the fibre bending experiments

2. The authors never state how they obtain stress and strain measurements. Do they know the exact fibre diameter for the individual experiment or do they use an average of their previous measurements? Is strain measured from the in situ images? Are their initial fiber lengths always the same? Otherwise, strain-at-fracture cannot be a fair comparative measure for ductility. Why is the elastic modulus considerably different between the model2 and model3 case? Model1 makes sense, based on the defects (voids,cracks) and maybe some residual organic template content, but I'm puzzled by the difference between 2 and 3.

Reviewer #4

(Remarks to the Author)
In this study, the authors demonstrate a crystalline/amorphous dual-phase TiO2 nanofiber that combines high strength, good flexibility, and room-temperature plasticity through an internal-interface regulation strategy. It is based on an innovative method for synthesizing ceramic nanofibers, which allows for impressive control over the growth and evolution of nanocrystals. Given the inherent brittleness and limited deformability of ceramic materials, such comprehensive optimization of their mechanical properties is both urgent and valuable, making this finding attractive. However, several aspects require further revision and clarification, such as how the micromechanical optimization of individual nanofibers influences the macroscopic properties. Overall, this work is interesting and possessing novelty, with well-structured content and coherent logic. I believe that, following the necessary revisions, this manuscript is worthy of consideration for publication in Nature Communications.

1. In the introduction, the authors discuss the potential for achieving plasticity in ceramics through the deliberate creation of crystal defects and cite related studies. However, they also claim that this approach may not be applicable to ceramic nanofibers (Lines 79-82). What is the basis for this assertion?

2. The development of a directly spinnable sol appears to be critical for achieving a dense structure in ceramic nanofibers. The manuscript notes that traditional methods for synthesizing ceramic nanofibers rely on polymer templates. Why does the LP-sol synthesize in this study exhibit spinnability? What is the origin for its spinnability? This point needs to be clarified.

3. For this work, the dual-phase configuration is essential for achieving the desired final structure. If the SP-sol were to aggregate, controlling the growth of nanocrystals would be highly challenging. In other words, how to ensure that SP-sol does not aggregate?

4. It is recommended to compare the crystallization behavior of Model-2 and Model-3 using XRD analysis. Additionally, Fig 2i does not indicate the sintering temperatures corresponding to the different curves.

5. In Section 2.4, I noticed that the authors provided videos for the in-situ tensile test of Model-1 and the in-situ bending test of Model-3. Please include additional videos that cover the in-situ tensile and bending tests for all models, to improve the completeness of the manuscript.

6. The authors emphasize the significance of enhancing the mechanical properties of individual fibers, noting that these properties determine the macroscopic mechanics of the nanofiber aggregate. However, the manuscript provides only limited demonstrations of this. I suggest further exploring the mechanical impact of single nanofibers on the aggregates they form to offer readers a more comprehensive understanding.

7. What is the bulk density of the aerogels shown in Fig 4m? What preparation method and raw materials were used? Were any additional components introduced? How does the mechanical performance compare to aerogels prepared from Model-1 and Model-2?

8. Compared to Model-3 (Lines 424-426), what is the electronic structure of Model-2? Does Model-2 also exhibit oxygen vacancies? Please provide this information. Could these differences be the key factor behind their plastic properties?

Version 1:

Reviewer comments:

Reviewer #1

(Remarks to the Author)
The authors have thoroughly addressed all the comments raised by both Reviewer #1 and Reviewer #2. The Molecular Dynamics (MD) section is now comprehensive and provides sufficient details to ensure reproducibility. Additionally, the authors have made significant revisions to the manuscript and the supplementary document in line with the reviewers' feedback and the authors' responses.

Upon reviewing the updated manuscript and the authors' responses, it can be concluded that all concerns have been adequately addressed. The revisions enhance the clarity and quality of the work, particularly in the simulation section, which now meets the necessary standards for scientific rigor and presentation.

We have no further comments or suggestions. We recommend the manuscript for acceptance in its current form.

Reviewer #2

(Remarks to the Author)
I co-reviewed this manuscript with one of the reviewers who provided the listed reports. This is part of the Nature Communications initiative to facilitate training in peer review and to provide appropriate recognition for Early Career Researchers who co-review manuscripts.

Reviewer #3

(Remarks to the Author)
The authors have taken my comments seriously and even conducted additional experiments. Therefore, my queries have been incorporated to a sufficient extent.

Reviewer #4

(Remarks to the Author)
It's acceptable for the current version.

Response to Reviewers

We sincerely appreciate the reviewers for their constructive feedback. These insightful and invaluable comments have significantly improved the quality and depth of the manuscript. According to the reviewers' suggestions and requirements, we have thoroughly revised the manuscript by conducting additional experiments and simulations, adding detailed methodological information, reorganizing related discussions, and providing specific clarifications. We hope these efforts will help elucidate our viewpoints and enhance the logical coherence of the study.

In the revised *Manuscript* and *Supplementary Information*, we have highlighted the changes in yellow. The following are point-by-point responses presented in blue.

Reviewer #1:

In this article, the authors have demonstrated that single ceramic nanofibers (CNFs) exhibit a good combination of high strength, superior deformability, and room temperature plasticity. This achievement is attributed to the optimized crystalline-amorphous dual-phase (DP) structure in CNFs, which includes reduced fiber defects and nanograin aggregation and increased crystalline-amorphous interfaces. The improved mechanical performance, opens up potential applications for CNFs in extreme scenarios such as mechanical shocks, high-frequency vibrations, and repeated twisting. The manuscript needs substantial revising and proper referencing. In addition, the supplementary figures are not discussed and poorly organized which can be improved for better understanding of the content. Hence, I would recommend the journal to publish this manuscript once the authors successfully revised the manuscript and addressed the following revisions/comments.

Response:

We sincerely thank the reviewer for the comprehensive and meticulous review, particularly for the valuable inspiration and guidance on MD simulations and mechanical mechanisms. Your positive feedback has been a great encouragement to us. In response to the reviewer's comments, we first focused on optimizing the MD simulations and verified the reliability and accuracy of the simulation results under different timestep conditions. Detailed information regarding the MD simulations has been thoroughly revised and polished, with appropriate citations of relevant references and comparative analyses between the simulation results and experimental findings. Subsequently, we deepened our understanding of the nucleation regulation and mechanical enhancement mechanisms of CNFs, providing relevant clarifications. Additionally, we organized a new "Discussion" section, which covers promising directions for further mechanical optimization of CNFs, particularly from the perspectives of EMTs and nanocrystal patterning design. Last but not least, we made substantial efforts to improve the writing by emphasizing clarity, logical flow, and precision to eliminate any ambiguity or unclear expressions, ensuring that the presented viewpoints are both clear and convincing. The visualization standards for all figures in the *Manuscript* and *Supplementary Information* have also been revised and unified. We hope these modifications and clarifications could fulfill the requirements and address the reviewer's concerns.

<u>Major Comment</u> #1:

Could the authors please explain their rationale behind selecting 1 fs as the timestep size and address any possible missing interactions or inaccuracies due to this choice? The size of the timestep in molecular dynamics simulations should, typically, be an order of magnitude smaller than the fastest motion time scale in the system. For TiO_2 modeled as flexible molecules with flexible bonds, the system has translational, vibrational, rotational, and torsional degrees of freedom (DOFs). Among these, the vibrational DOF is the fastest, with a typical time scale of ~1 fs. At high temperatures, such as 3300 K, this motion becomes even more significant due to the elevated kinetic energy of the atoms. Therefore, to capture high-accuracy interactions, an optimal timestep should be less than 1 fs, unless otherwise specific reasons are mentioned. Is there a convergence test? Or is this to minimize round-off errors? For reference, a previous study (J. Phys. Chem. C 2007, 111, 19, 6920–6926) used a 0.5 fs timestep for simulating TiO_2.

Response:

We thank the reviewer for raising concerns regarding the timestep size in MD simulations, and we appreciate the opportunity to clarify this matter. At the early stages of this study, we reviewed and learned from relevant studies, trying to construct rational models for metal oxides (*e.g.*, *AIP Adv.* **2023**, 13, 085226; *J. Chem. Phys.* **2015**, 142, 234102; *J. Stat. Phys.* **2015**, 160, 1696; *Chinese Phys. B.* **2019**, 28, 103102; *Npj Comput. Mater.* **2018**, 4, 59; *Nature* **2022**, 606, 909). The timestep sizes employed in these studies were typically set to 1.0-2.0 fs. In order to balance accuracy and computational efficiency, part of these computational setups were learnt and adopted in this work. However, as you pointed out, the timescale of the vibrational DOF is quite fast in our case (TiO_2 system). According to Nyquist's theorem, the timestep must be half or less than the fastest kinetic cycle. Additionally, the high-temperature conditions involved in the modelling process would lead to elevated atomic kinetic energies, necessitating a reliability assessment of the selected timestep size.

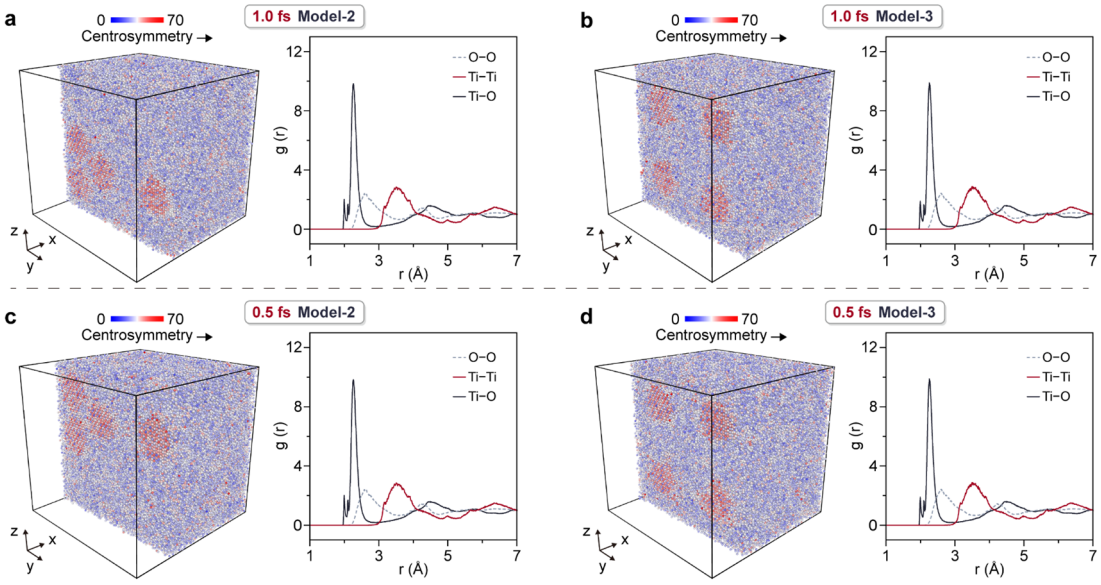

Revision Fig. 1. MD models constructed under different timestep conditions, with corresponding radial distribution function (RDF) curves obtained for comparison. (a) Model-2 (1.0 fs), (b) Model-3 (1.0 fs), (c) Model-2 (0.5 fs), (d) Model-3 (0.5 fs).

Hence, by thoroughly considering the comments and references (*J. Phys. Chem. C* **2007**, 111, 6920) provided by the reviewer, we decided to rerun the MD simulations using a more precise timestep (0.5 fs) to verify the accuracy of our computational results. The comparison indicates that the results obtained with timestep size of 0.5 fs and 1.0 fs were consistent (**Revision Fig. 1** and **Revision Fig. 2**), including the model structures, corresponding RDF curves, and fracture positions under tensile loading. These findings confirm the reliability of our initial simulations. Additionally, we have revised the relevant sections in the *Manuscript* and *Supplementary Information* to incorporate these updates.

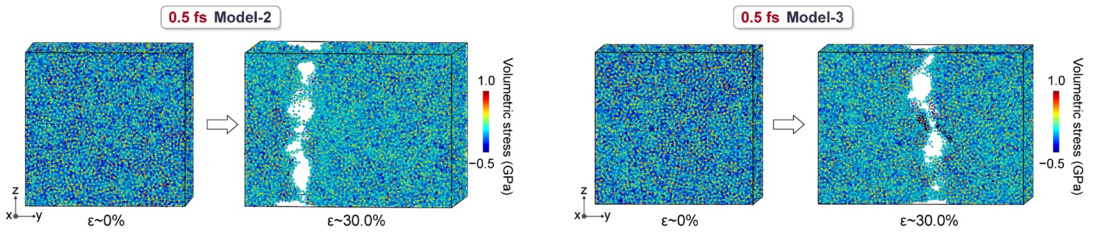

Revision Fig. 2. MD tensile simulation results for Model-2 and Model-3, performed with a timestep of 0.5 fs along the y-axis to verify the results.

- **Revisions to *Section 4.5* in the Manuscript**

Following energy minimization, the structures were optimized using two NVT ensembles at 300 K and 3300 K, regulated by a Nose-Hoover thermostat. To ensure accuracy and reproducibility, timesteps of 1.0 fs and 0.5 fs were both tested during the simulations. The NVT optimization process was conducted for 100 ps to achieve stable structures.

- **Revisions to *References* in the Manuscript**

33. Luan B, Huynh T, Zhou R. Simplified TiO_2 force fields for studies of its interaction with biomolecules. *J. Chem. Phys.* **142**, 234102 (2015).
34. Zhang S, Wu Y. Investigating the crystallization behavior of TiO_2 during annealing: molecular dynamics simulations. *AIP Adv.* **13**, 085226 (2023).
35. Koparde VN, Cummings PT. Molecular dynamics study of water adsorption on TiO_2 nanoparticles. *J. Phys. Chem. C.* **111**, 6920 (2007).

- **Revisions to *Supplementary Fig. 1***

The initial TiO_2 models were constructed based on the mp-390 structure as the minimum periodic unit, with dimensions of 12.32 nm × 12.32 nm × 11.84 nm. In these models, atomic positions within eight nanospheres, each with a radius of 1.75 nm, were fixed. The remaining atoms were randomly displaced in the x, y, and z directions, with a maximum displacement of 0.2 nm in each direction, to form an amorphous structure containing eight grains. Consequently, an amorphous matrix containing eight nanograins was obtained. Two distinct models were created based on the distribution of nanospheres: a uniform (non-aggregated) distribution and a non-uniform (aggregated) distribution. For each simulation, energy minimization was first performed to relax the simulation box. Subsequently, two NVT ensembles were used to optimize the structure, with timesteps of 1.0 fs and 0.5 fs both carefully tested. The temperatures were set to 3300 K and 300K, respectively, and controlled using a Nose-Hoover thermostat. The NVT optimization process was run for 100 ps to achieve stable structures.

<u>Major Comment</u> #2:

MD simulation methodology section (*Section 2.1*: Conceptual design) is not comprehensively written and lacks proper referencing. For example, in pg. 5, "By employing the Large-scale Atomic/Molecular Massively Parallel Simulator (LAMMPS) and the Matsui-Akaogi force field, we obtained amorphous and DP TiO_2 models (Fig. 1c and 1d)." Here, references to LAMMPS code and the force field are missing. Additionally, how the following line—"Then, the tensile simulations were performed on box models (147455 atoms) with a strain rate of 10^9 s^{-1} along the x-axis (Fig. 1f and 1g)[33, 34]"—is related to the cited Refs. 33 and 34.

Response:

We fully agree with the reviewer that the manuscript would benefit from a more comprehensive description of the MD simulation methodology, which would enhance its reproducibility and readability. We would like to draw the reviewer's attention to the revisions made in *Section 2.1* and *Section 4.5* of the manuscript, where more detailed information and references have been added to describe and cite the related LAMMPS methods and Matsui-Akaogi force fields. Additionally, we have sorted out the logic of the tensile simulations, and updated several references to ensure they are more directly relevant to the tensile simulations in this study. Furthermore, all computational details have been consolidated into the description provided in **Supplementary Fig. 1**.

- **Revisions to *Paragraph 3 of Section 2.1* in the Manuscript**

We utilized LAMMPS and the Matsui-Akaogi force field to construct various TiO_2 models, including amorphous and DP structures (Fig. 1c and 1d). The Matsui-Akaogi force field has been validated as one of the most appropriate for describing TiO_2 (details provided in the description of Supplementary Fig. 1)[33, 34, 35]. In the radial distribution function (RDF) of DP TiO_2, peaks located at ~ 1.99 Å in the Ti−O curve, and at ~ 3.15 Å and ~ 3.89 Å in the Ti−Ti curve, highlight its hypocrystalline features (Fig. 1e). For different DP configurations, Model-2 represents nanocrystal aggregation, whereas Model-3 features uniformly distributed nanograins. Tensile simulations were then performed on Model-2 and Model-3 to investigate differences in their mechanical behaviors[6, 27, 36, 37].

- **Revisions to *Section 4.5* in the Manuscript**

The MD simulations were performed using LAMMPS[71], with the Matsui-Akaogi force field employed[33, 34, 35]. This force field accounts for two key contributions: (i) electrostatic interactions (partial charges of +2.196 for Ti and −1.098 for O) and (ii) van der Waals interactions (expressed via the Buckingham potential). The DP TiO_2 models were constructed with dimensions of 12.32 nm × 12.32 nm × 11.84 nm, embedding eight nanocrystals, each with a radius of 1.75 nm. Distinct configurations of DP models were created based on the nanograin distribution: uniform and aggregated arrangements. Following energy minimization, the structures were optimized using two NVT ensembles at 300 K and 3300 K, regulated by a Nose-Hoover thermostat. To ensure accuracy and reproducibility, timesteps of 1.0 fs and 0.5 fs were both tested during the simulations. The NVT optimization process was conducted for 100 ps to achieve stable structures. Subsequently, uniaxial tensile simulations were performed by extending the simulation box along the x-axis at a strain rate of 1×10^9 s^{-1} to examine the mechanical behavior[6, 27, 36, 37]. Atomic motions were calculated using the Velocity-Verlet algorithm. Additional details are provided in the in the description of Supplementary Fig. 1.

- **Revisions to *Supplementary Information***

Supplementary Fig. 1. MD models and tensile simulation details. Structural representations of Model-2 and Model-3, including sliced views to reveal internal details, were used for tensile simulations along the x-axis. The color scale bar represents the centrosymmetry parameter of each atom in the simulated system.

MD simulations were conducted using the Large-scale Atomic/Molecular Massively Parallel Simulator (LAMMPS, version 23 Jun 2022)[1]. The Matsui-Akaogi force field, widely recognized as one of the most suitable force fields for TiO_2 solids (including both crystalline and amorphous structures), was employed to describe atomic interactions in the TiO_2 models used in this study[2, 3, 4, 5]. This force field incorporates two key contributions: (i) electrostatic interactions (q_iq_j/r_{ij}) and (ii) van der Waals interactions, expressed in the Buckingham potential form[6]. The interaction energy U between atoms i and j separated by a distance r_{ij} is given by:

$$U(r_{ij}) = A_{ij}\exp\left(-\frac{r_{ij}}{\rho_{ij}}\right) - \frac{C_{ij}}{{r_{ij}}^6} + \frac{q_iq_i}{r_{ij}}$$

Here, r_{ij} denotes the interatomic distance, and q_{ij} represents the critical shielding length, while A_{ij} and C_{ij} are the strength parameters for repulsive and attractive dipole-dipole

interactions, respectively[7]. For electrostatic interactions, this force field assigns partial charges of +2.196 for Ti and −1.098 for O. The Buckingham potential incorporates contributions from the Born-Mayer repulsion potential and dipole-dipole interactions, with the specific parameters outlined below:

Interaction	A_{ij} (kcal mol^{-1})	ρ_{ij} (Å)	C_{ij} (kcal mol^{-1} Å^{-1})
Ti−Ti	717654	0.154	120.997
Ti−O	391053	0.194	290.392
O−O	271719	0.234	696.941

The initial TiO_2 models were constructed based on the mp-390 structure as the minimum periodic unit, with dimensions of 12.32 nm × 12.32 nm × 11.84 nm. In these models, atomic positions within eight nanospheres, each with a radius of 1.75 nm, were fixed. The remaining atoms were randomly displaced in the x, y, and z directions, with a maximum displacement of 0.2 nm in each direction, to form an amorphous structure containing eight grains. Consequently, an amorphous matrix containing eight nanograins was obtained. Two distinct models were created based on the distribution of nanospheres: a uniform (non-aggregated) distribution and a non-uniform (aggregated) distribution. For each simulation, energy minimization was first performed to relax the simulation box. Subsequently, two NVT ensembles were used to optimize the structure, with timesteps of 1.0 fs and 0.5 fs both carefully tested. The temperatures were set to 3300 K and 300K, respectively, and controlled using a Nose-Hoover thermostat. The NVT optimization process was run for 100 ps to achieve stable structures.

Following the NVT simulation, the mechanical behaviors of the TiO_2 system under uniaxial tensile were studied[8, 9, 10, 11], by elongating the simulation box along the x-axis at a strain rate of 1×10^{9} s^{-1}. In all MD simulations, atomic motion was described using the classical Newton's equation, and solved with the Velocity-Verlet algorithm.

Major Comment #3:

Did the authors quantify the nanocrystals within the amorphous matrix? A measure of a quantification, say volume fraction of nanocrystals, in Model-2 and Model-3 can help comprehend the role of such nanocrystals in enhancing strength and ductility. Is it possible that from Model-1 to Model-3, the improvement can be explained with the Rule of Mixtures? If not, then can other effective medium theories (EMTs)–Maxwell (can be thought as Model-3) or Rayleigh (Model-2)–be utilized to explain the observed results?

Response:

The volume fraction of each component within a ceramic material often plays a pivotal role in determining its properties. As the reviewer mentioned, quantifying nanocrystals can provide valuable insights into the mechanical behavior of CNFs. Based on the MD model parameters, the nanocrystal volume fractions for both Model-2 and Model-3 were calculated to be ~9.99%. This is because, aside from the distribution of nanocrystal spheres, Model-2 and Model-3 possess identical parameters, including model dimensions, the amorphous matrix, nanocrystal sphere size and quantity, and RDF curves. In this scenario, the primary factor contributing to the differences in mechanical properties between Model-2 and Model-3, is the spatial distribution of the dual-phase structure, which is the central focus of this study. This difference was confirmed through structural characterizations, as both models exhibited similar crystallinity (**Manuscript Fig. 3f**) and average grain size (**Manuscript Fig. 3g**), yet distinct nanocrystal aggregation morphologies (**Manuscript Fig. 3e**). In light of these considerations, the Rule of Mixtures may not be highly applicable to the focus of this work. This rule is commonly used to predict the modulus and strength of composites, on the basis of the weighted contributions of inclusions and matrices (*J. Mech. Phys. Solids* **1964**, 12, 199). One of its key assumptions is that certain macroscopic properties of a composite material are weighted averages of the properties of its constituent materials. Accordingly, it is primarily factoring in the percentage (by volume, mass, or concentration) of each component. However, it is difficult to figure out the material property variations arising from identical component ratio yet different spatial distributions.

Inspired by the reviewer's insights, we sought to further explore other EMTs to better understand the findings of this work. Among these, the "Maxwell" theory is a

classical model widely used to describe the effective mechanical or thermal properties of composites with low volume fractions of dispersions (*Mech. Mater.* **2014**, 75, 45; *J. Power Technol.* **2015**, 95, 14; *Int. J. Eng. Sci.* **2019**, 140, 35). In this theory, dispersions are typically assumed to be uniformly-distributed spherical particles with no interactions among them. While the model is applicable only to low dispersion volume fractions, and takes no account of particle interactions, it may still partially describe Model-3 under certain conditions. For instance, in analyzing the effects of nanograin size or quantity on the mechanical properties of Model-3, it may yield rational predictive results under specific assumptions. However, the "Maxwell" theory is likely inapplicable to Model-2, as the aggregated nanocrystals require consideration of mutual interactions and interference among particles. Additionally, for dual-phase TiO_2, chemical bonding at the crystalline/amorphous phase interface introduces chemical interactions that EMTs do not account for, as they are generally based on physical contact. Consequently, the "Maxwell" theory has limitations in accurately describing Model-3 and the mechanical differences arising from variations in nanocrystal distributions.

The "Rayleigh" theory has also been demonstrated to effectively describe the properties of multicomponent composites, such as thermal and electrical conductivity. Notably, the "Rayleigh" theory includes the mutual interaction of dispersions in its equations (*J. Power Technol.* **2015**, 95, 14), potentially making it more suitable than the "Maxwell" theory for describing Model-2. However, it is important to note that this theory also does not account for chemical bonding at the phase interface or the evolution of such interactions. At smaller scales, the amorphous and crystalline regions are interconnected and "glued" by chemical bonds, contributing to complex deformation mechanisms such as bond switching (*Nat. Commun.* **2010**, 1, 24; *Nano Lett.* **2016**, 16, 105; *Science* **2019**, 366, 864; *Science* **2022**, 378, 371) and grain rotation (*Science* **2024**, 386, 49), which should not be simplified in mechanical understanding. Consequently, while these EMTs enrich perspectives on the mechanics of CNFs, they may not be entirely sufficient.

We thank the reviewer for the insightful perspectives, which have been invaluable in deepening our understanding of the findings in this study. After careful consideration, we propose to revise the original "Conclusion" section into a "Discussion" section, incorporating additional paragraphs to address the EMT perspectives raised.

- **Revisions to *Discussion* in the Manuscript**

One potential avenue is utilizing Model-3 as a platform to systematically modulate the size and quantity of nanograins (Supplementary Fig. 26), thereby gaining insights into how the volume fraction of the nanocrystal domain affects the evolution of the DP structure under loading. Accelerating this process could benefit from the incorporation of effective medium theories[70]. With appropriate modifications, these classical theories are expected to simplify structure-mechanics relationships and offer predictive and guiding information. Another promising direction lies in the patterned design or orderly arrangement of nanocrystal regions within amorphous matrices. A more ordered and uniform distribution is predicted to suppress shear-band activation, and meanwhile constrain the migration and bypassing of disordered atomic clusters, thereby further promoting the mechanical strength and strain limits[27].

- **Revisions to *Supplementary Information***

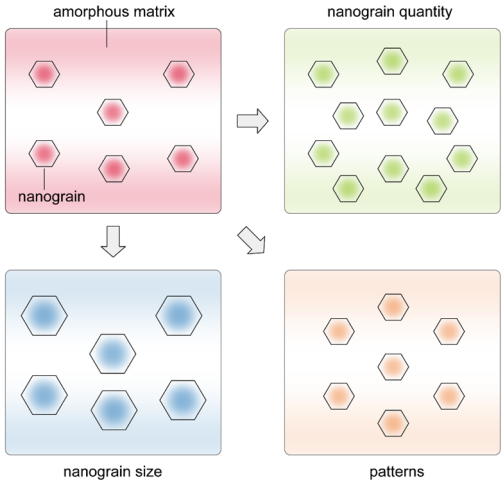

Supplementary Fig. 26. Promising directions for further improving the comprehensive mechanical properties of DP CNFs.

<u>Major Comment</u> #4:

The manuscript, especially the "structural analysis" section (Section 2.3), lacks coherency and purpose of the analyses conducted. Here are some examples:

Response:

We sincerely thank the reviewer for pointing out these issues, which are critical for improving the quality of the manuscript. Accordingly, we have made the necessary revisions to the "Structural Analysis" section (*Section 2.3*) to achieve better consistency and clearer purpose.

a) Pg. 11: "Their diameters were aligned to exclude size-dependent interference (Supplementary Fig. 13)." Here, supplementary Fig. 13 does not contain any quantitative information on diameters.

We would like to draw the reviewer's attention to the insets in **Fig. 3b** of the original manuscript, which present statistical data on the diameters of CNFs. To further improve clarity, we have moved these quantitative statistics in *Supplementary Information*.

- **Revisions to *Supplementary Information***

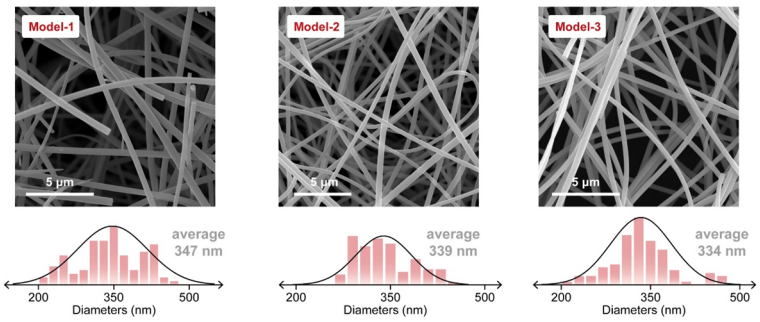

Supplementary Fig. 13. Morphology of CNFs obtained from different sols. SEM images and diameter statistics of DP TiO_2 nanofibers fabricated from SP-sol, LP-sol, and binary sols are presented for comprehensive comparison, labeled as Model-1, Model-2, and Model-3. Their diameters were regulated to exclude size-dependent interference.

b) Pg. 11: "Additionally, calculations based on the Langmuir theory verify the same tendency." Here, the tendency is not discussed clearly and the statement is vague. Also, no citation to Langmuir theory for readers is provided for completeness.

We have reorganized the relevant descriptions and added citations for the references related to Langmuir and BET theories.

- **Revisions to *Paragraph 1 of Section 2.3* in the Manuscript**

The specific surface area calculated from BET theory is based on the multilayer gas adsorption model. For verification, Langmuir theory, which assumes monolayer gas adsorption[62, 63], was also applied. The Langmuir surface area results show the same trend, with Model-1 exhibiting a notably larger surface area than Model-2 and Model-3, consistent with the BET findings.

- **Revisions to *References* in the Manuscript**

62. Shimizu S, Matubayasi N. Surface area estimation: replacing the Brunauer–Emmett–Teller model with the statistical thermodynamic fluctuation theory. *Langmuir* **38**, 7989 (2022).

63. Shimizu S, Matubayasi N. Understanding sorption mechanisms directly from isotherms. *Langmuir* **39**, 6113 (2023).

c) Pg. 11: "… and micropores in Model-1 may serve as the weakest link to CNF fracture (Fig. 3d). Sintering is a crucial …" Here, sentences and transitions lack coherency and consistency.

The related paragraphs have been modified to improve clarity and consistency. Please see the following:

- **Revisions to *Paragraph 1 of Section 2.3* in the Manuscript**

Compared to the non-porous structures of Model-2 and Model-3, the mesopores and micropores in Model-1 would serve as the weakest link (Fig. 3d), rendering it more prone to fracture under load. These porosities predominantly form during the sintering stage of the CNFs, driven by the evolution of constituents and structural defects. Thus, we further examined the sintering process through thermoanalytical methods.

d) How the supplementary Fig. 15 explains the weight loss of Model-1 is not discussed. The text: "In addition, a counterintuitive rising- plunging trend observed between 438.84-509.11 °C may result from deep residual carbon oxidation and consequent gas release." What is the purpose of this sentence and supplementary Fig. 15c?

The original **Supplementary Fig. 15** has been revised. We have added an explanation for Model-1's weight loss and would like to draw the reviewer's attention to the updated **Supplementary Fig. 15** and its descriptions.

The original **Supplementary Fig. 15c**, which presented the first-order derivative of the TG (DTG) curve, was included to illustrate the rate of CNF weight change as a function of temperature during the sintering process. Sharp peaks observed in the DTG curve help explain the compositional evolution at each stage.

Due to insufficient transitions and explanations, the purpose of the sentence, "In addition, a counterintuitive rising-plunging trend observed between 438.84-509.11 °C..." may have appeared ambiguous. This statement was intended to indicate that "oxidation of residual carbon and subsequent gas release may be one of the key reasons for structural defects in Model-1." We have rephrased the relevant paragraph and incorporated schematic illustrations of the CNF structural evolution mechanism into **Supplementary Fig. 15** to clarify this point.

- **Revisions to *Paragraph 1 of Section 2.3* in the Manuscript**

Between 438.84 °C and 509.11 °C, a rising-plunging trend is observed in the TG curve of Model-1, which could be attributed to the oxidation of residual carbon and subsequent gas release. As the gases diffuse and escape, they would leave behind pathways to behave as structural defects. Furthermore, Model-1 exhibits weight loss termination at ~538.44 °C, markedly later than Model-2 (~344.15 °C) and Model-3 (~339.35 °C).

- **Revisions to *Supplementary Information***

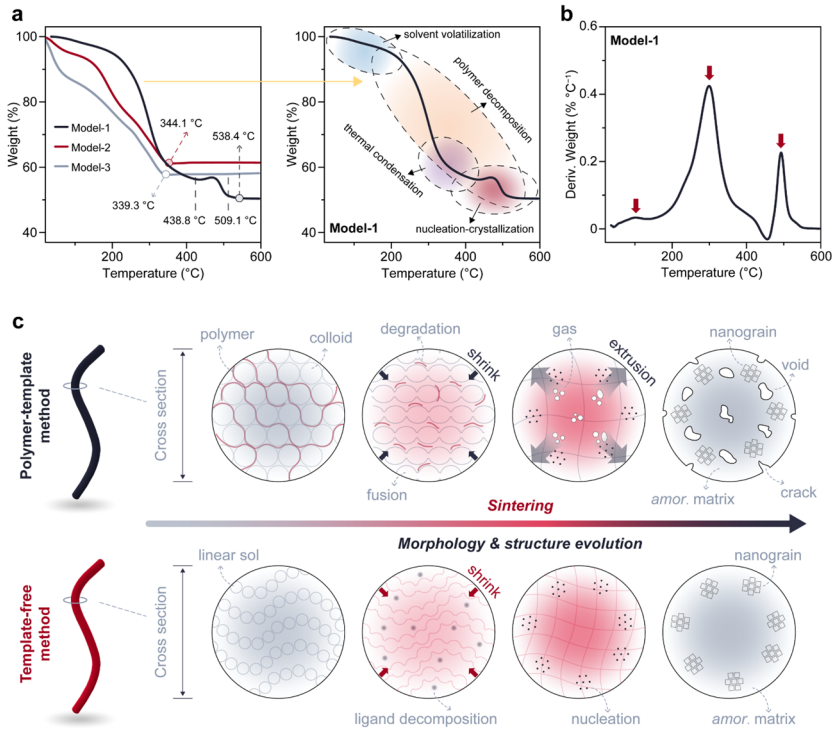

Supplementary Fig. 15. Thermoanalysis of Model-1, Model-2, and Model-3 during sintering. (a) TGA curves of Model-1, Model-2, and Model-3. The complex weight loss behaviors of Model-1, including solvent volatilization, thermal condensation, polymer decomposition, and nucleation-crystallization processes. (b) The first-order derivative of the TGA curve (DTG curve) for Model-1. (c) Schematic representation of the structural evolution of CNFs fabricated via polymer-template and template-free electrospinning methods during the sintering process.

The component and structural evolution during CNF sintering was analyzed. The weight loss of Model-1 up to ~200 °C is primarily attributed to the evaporation of solvents such as ethanol, butanol, and water. Although butanol was not directly used during the preparation, it forms via the hydrolysis of Ti alkoxide (–Ti–OBu + H_2O → –Ti–OH + BuOH). A minor mass loss peak at ~105 °C in the DTG curve reflects the rapid escape of solvents, as these molecules are deeply embedded in the precursor fibers and interact with the polymer and Ti–O crosslinked network, requiring higher temperatures for removal. Another notable mass loss peak appears between 200-400 °C, mainly due to the thermal decomposition of the polyvinylpyrrolidone (PVP) template, which involves the breaking of polymer chains and their decomposition into small molecules[24]. Organic residues often remain at this stage. A shoulder peak at ~350 °C indicates thermal polycondensation, where retained –Ti–OH groups condense (–Ti–OH + –Ti–OH → –Ti–O–Ti– + H_2O), causing further mass loss. After ~370 °C, nucleation and crystallization commence, while residual carbon undergoes oxidation and releases gases (439-509 °C), leaving diffusion pathways that subsequently form structural defects in the CNFs.

<u>Major Comment</u> #5:

In Figure 1g, could the authors include strain values in addition to the number of steps? It appears that Model-2 and Model-3 undergo crack/void nucleation after 18.2×10^4 and 47×10^4 steps, respectively. This indicates that Model-2 and Model-3 experience cracks at applied strain values of 18.2% and 47%, respectively, given that timestep size = 1 fs, strain rate = 10^{-9} s^{-1}, and strain applied at every step (dynamic stretching). Could the authors please clarify how these simulation strain values can be compared with experimentally-obtained strain values (e.g., σ¬u and σ¬f)?

Response:

We appreciate the reviewer's suggestion to label the strain values in **Fig. 1g** of the manuscript, and the figure has been revised accordingly. We would like to explain that the total steps in the MD simulation include those from the relaxation process (20×10^4 steps, 100 ps for two NVT optimization, respectively). When calculating strain, these relaxation steps need to be subtracted, indicating that the tensile simulation begins after the 20×10^4 step. In the original **Fig. 1g**, the steps for Model-2 were labeled correctly, as the relaxation steps had already been subtracted. However, the steps in Model-3 were labeled incorrectly, as they did not account for the subtraction of relaxation steps. The correct values should be 27×10^4 steps and 35×10^4 (47×10^4–20×10^4 and 55×10^4–20×10^4, respectively). We apologize for any resulting misinformation or confusion.

- **Revisions to *Fig. 1g* in the Manuscript**

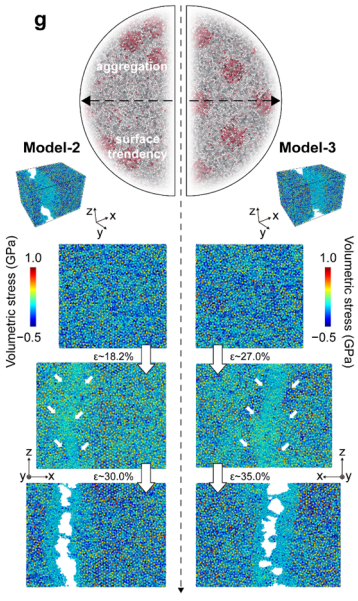

Fig. 1. (g) Tensile simulations of Model-2 and Model-3.

Regarding the strain calculation, your procedure is correct. During the tensile process, Model-2 reaches a strain of 18.2% after 18.2×10^4 steps, while Model-3 corresponds to a strain of 27.0% after 27.0×10^4 steps. These high-strain snapshots were selected to highlight the fracture locations. Based on the MD simulation results, the stress-strain curves for Model-2 and Model-3 were obtained (**Revision Fig. 3**).

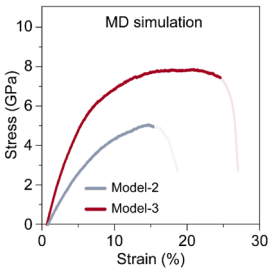

Revision Fig. 3. The extracted stress-strain curves based on MD simulations.

It is important to note that deviations indeed exist between the absolute strain values obtained from MD tensile simulations and single-CNF tensile experiments, primarily due to the following factors. First, the cross-sectional area of the MD simulation model is significantly smaller than the actual size of the experimentally-prepared CNFs. Due to the tremendous computational challenges of simulating huge submicron-scale MD models (with Model-3 having an average diameter of ~334 nm), it is reasonable and common in similar studies (*Nature* **2022**, 606, 909) to use small equivalent models to capture atom-scale behaviors and intrinsic mechanisms that are difficult to observe experimentally. These size differences may cause the simulated absolute strain values to deviate from experimental data. Second, MD simulations are typically conducted at a much faster strain rate (1×10^9 s^{-1}) compared to the experimental tensile rate of 5 nm s^{-1}, which further contributes to these deviations. Lastly, MD models are idealized, whereas it is nearly impossible to perfectly avoid any tiny defects in experimental samples, meaning that the practical CNFs can hardly achieve such an idealized condition. Hence, these mentioned factors may limit the practical samples to reach the idealized strain limit values.

Although there are deviations in absolute strain values, the MD simulations and experiments exhibit consistent trends in the stress-strain curves, such as Model-3 achieving a higher strain limit than Model-2. This consistency demonstrates that MD simulations are valuable and reliable for revealing contrastive differences in the mechanical properties of materials. Moreover, MD simulations allow us to observe subtle atomic-scale changes occurring in CNFs during tensile stretching, which are

challenging to capture directly in experiments. Furthermore, the simulations highlight differences in fracture location and associated mechanisms, providing further insights into the fracture behavior of CNFs with different dual-phase distributions.

<u>Major Comment</u> #6:

Did the authors compare the stress-strain curves obtained from push-to-pull (PTP) experimental setup with those obtained from MD simulations? Figure 4c presents the experimentally-extracted stress-strain response, but it is unclear as to how well or poorly the MD-computed stress-strain response curve agrees with the former ones.

Response:

We have provided a comparison of the stress-strain curves obtained from MD simulations and single-CNF tensile experiments (**Revision Fig. 4**). Indeed, there are deviations between the absolute values obtained from MD tensile simulations and experimental tests, particularly in terms of ultimate strength and strain limits. As outlined in our response to Comment #5, these deviations can be attributed to several factors, including differences in size between the MD models and experimental samples, disparities in strain rates, and the idealized nature of MD models. Additionally, we observed a "tail" in the MD stress-strain curves, which is absent in the experimental data. This occurs because, in practical experiments, the interaction between the two fractured segments of the fiber ceases immediately upon breakage. In contrast, MD simulations retain some degree of interaction even the fracture begins, resulting in the observed tail.

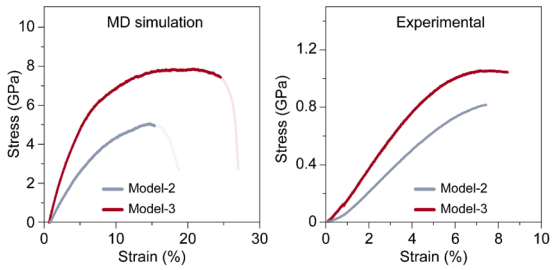

Revision Fig. 4. The extracted stress-strain curves based on MD simulations (left) and single-CNF tensile experiments (right).

These are inherent limitations of MD simulations. Nevertheless, it is important to emphasize that the MD and experimental stress-strain curves exhibit consistent trends, such as the higher strength and strain limits observed in Model-3 compared to Model-2. This consistency highlights the value and reliability of MD simulations in revealing the relative mechanical performance of different material structures. The primary objective of the MD simulations is to observe subtle atomic-scale changes in CNFs

during tensile deformation, which are difficult to capture directly through experiments. Moreover, MD simulations provide critical insights into the fracture initiation points of CNFs. Overall, our aim is to use MD simulations to complement experimental and characterization results, thereby offering a deeper understanding of the corresponding fracture mechanisms.

Major Comment #7:

The authors claim that dangling bonds enhance feasibility: "The presence of numerous oxygen vacancies in Model-3 suggests the presence of dangling bonds, thus chemically supporting the feasibility (Fig. 4i)[62]." Here, can the authors define "feasibility" and clarify how the presence of dangling bonds enhance such feasibility? If it is about the bond switching phenomenon, then did the authors observe any bond switching in this case?

Response:

As noted by the reviewer, the "feasibility" is indeed referred to "the occurrence of bond-switching events". Frankberg *et al.* (*Science* **2019**, 366, 864) reported the plastic deformation behavior of metal oxides initiated by bond switching. Their study demonstrated that the deformation of materials under shear and tensile loading becomes more diverse due to bond switching and rotation. They concluded that the plasticity observed in Al_2O_3 likely depends on the accumulation of bond-switching events in localized atomic groups. During deformation, the central Al atom can move into an adjacent space, forming a new bond with an O atom to replace the original bond. Furthermore, such bond-switching events have also been observed in other studies investigating the plastic behavior of amorphous or dual-phase ceramic materials (*Nano Lett.* **2016**, 16, 105; *Science* **2022**, 378, 371).

On the other hand, in terms of promoting bond-switching events by vacancies and dangling bonds, Zhang *et al.* (*Nat. Commun.* **2010**, 1, 24) reported a strategy that involves inducing numerous oxygen vacancies and dangling bonds via high-energy electron beam treatment to improve the ductility of oxide ceramics. During deformation, these dangling bonds recombine with neighboring atoms, accompanied by the rotation and migration of associated atomic groups. Such artificially induced dangling bonds and vacancies are recognized to help overcome energy barriers and facilitate the initiation of bond switching. The repetition and accumulation of these bond-switching events ultimately support the plasticity of the material. As shown in **Revision Fig. 5**, a broken bond creates a dangling silicon bond and a non-bridging oxygen atom. The non-bridging oxygen then bonds with a different silicon atom, simultaneously causing this silicon to sever its bond with another oxygen. Consequently, the SiO_4 unit clusters undergo rotation and relocation.

[figure redacted]

Revision Fig. 5. The representative bond-switching event in SiO_2. Copyright 2010, Springer Nature. (*Nat. Commun.* **2010**, 1, 24)

In view of these insights, it is reasonable to speculate, as stated in the original manuscript, that some degree of bond-switching events could occur during the deformation of CNFs, aligning with findings from studies on metal oxides. The intrinsic oxygen vacancies in Model-3, as evidenced by XPS, along with the resulting dangling bonds, would play an essential role in facilitating these bond-switching events (as the absence of adjacent O atoms could make the central Ti atoms more susceptible to movement). The accumulation of such bond-switching events is one of the key factors that enables the deformations in the CNFs.

We have modified the sentence "The presence of a large number of oxygen vacancies in model-3 suggests..." for better accuracy and readability:

- **Revisions to *Paragraph 4 of Section 2.4* in the Manuscript**

The XPS O1s spectra reveal the presence of oxygen vacancies in Model-3, implying a number of dangling bonds within the structure (Fig. 4i and Supplementary Fig. 24)[67]. It is reported that the bond-switching events can be initiated by these vacancy defects and dangling bonds, which are beneficial in improving the deformation potential of oxide ceramics[68, 69].

Major Comment #8:

In Model-3, is it the nanocrystal regions that help with the ductility or the amorphous matrix? The text: "Importantly, the amorphous matrix gains improved structural continuity and an increased internal interface, acting as a soft boundary to efficiently transfer and dissipate stress. These multiple deformation mechanisms encourage the fracture of CNFs to occur after plastic deformation. Eventually, as shown in Fig. 1g, Model-3 may fracture due to localized stress concentration in shear bands within the amorphous regions, rather than initiating in the nanocrystal domains[26, 35, 36, 37]." Model-1 and Model-3 both contain shear bands in the amorphous matrix and the only difference is that in Model-3, there are nanocrystals that can act as hindrance to shear bands. So, it seems like that the presence of nanocrystals help with the ductility and strength. Can the authors clarify?

Response:

We appreciate the opportunity provided by the reviewer to clarify this point. In this study, we actually proposed three crystalline/amorphous dual-phase CNF models for comparison (**Revision Fig. 6a**). Specifically, Model-1 was prepared using the conventional method, resulting in a non-dense structure with cracks, voids, and pores due to methodological limitations. Model-2, on the other hand, was prepared using a newly designed template-free method, effectively eliminating these structural defects. Building on this, the dual-phase configuration was optimized to obtain Model-3, which avoided nanograin aggregation. According to the tensile testing results (**Revision Fig. 6b**), the comprehensive mechanical properties of Model-1 were notably inferior to those of Model-2 and Model-3. The structural defects on Model-1, as the weakest link, are prone to stress concentration under tensile loading and leading to catastrophic fractures. Hence, the significant increase in strength and ductility of model-3 over model-1 can be attributed to the elimination of structural defects and the optimization of the dual-phase configuration.

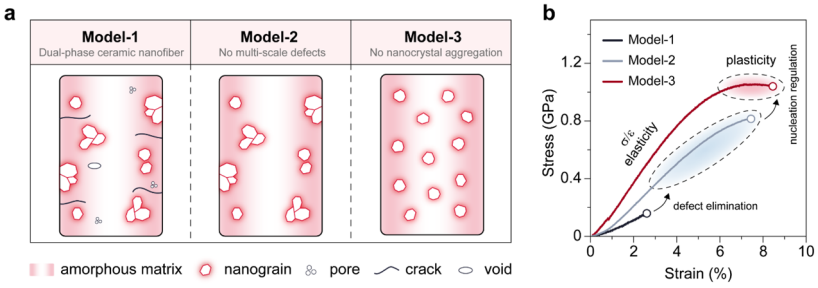

Revision Fig. 6. (a) Structural schematics of different dual-phase CNFs. (b) Corresponding tensile stress-strain curves for the CNFs.

To explain the simultaneous improvement of ductility and strength observed in Model-3, it is necessary to comprehensively analyze the fracture mechanisms of CNFs with different crystal structures (**Revision Fig. 7**). (i) Crystalline CNFs typically exhibit a polycrystalline structure characterized by numerous grain boundaries. During tensile deformation, these grain boundaries are prone to slip and tearing, where the cracks would occurs and rapidly extend, ultimately resulting in brittle fracture. (ii) Amorphization has overcame this issue to some extent for CNFs, because of the absence of obvious grain boundaries. The fracture of amorphous ceramics is generally initiated by the activation and development of shear bands. However, due to the simplistic and homogeneous structure of amorphous CNFs, the initiation of shear bands is random and unconstrained, which limits further mechanical enhancement. (iii) In this regard, Model-3, with its dual-phase structure comprising nanocrystals embedded within an amorphous matrix, demonstrates significant advantages. The uniformly distributed nanocrystal regions could help stabilize the surrounding disordered atomic clusters (*Ceram. Int.* **2019**, 45, 19845; *Nature* **2022**, 606, 909; *Nat. Mater.* **2023**, 22, 42), thereby enhancing the strength and modulus of CNFs. Additionally, the interaction between the nanocrystals and the amorphous matrix would encourage multiple deformation mechanisms, such as bond-switching (*Nat. Commun.* **2010**, 1, 24; *Nano Lett.* **2016**, 16, 105; *Science* **2019**, 366, 864; *Science* **2022**, 378, 371) and grain rotation (*Science* **2024**, 386, 49), which dissipate stresses and delay shear-band activation until a higher tensile strain threshold is reached. Although both Model-3 and its amorphous counterpart are expected to fracture via the development of shear bands, the dual-phase configuration in Model-3 could enable a more stable structure and diverse deformation modes, rendering higher tensile strength and strain limits.

Hence, as the reviewer noted, the primary difference between Model-3 and its amorphous counterpart lies in the presence of nanocrystals. From this perspective, these nanocrystals help stabilize the amorphous matrix and inhibit shear band formation, thereby enhancing both strength and ductility. But on the other hand, compared to polycrystalline counterparts, the ductility of Model-3 primarily originates from its continuous amorphous matrix. Besides, it is worth noting that the fracture of Model-1 can be attributed to the stress concentration and crack extension caused by inherent

fiber defects, leading to failure before the shear-band mechanism is activated. In light of above analysis, particularly the differences between Model-2 and Model-3 discussed in the manuscript, we believe that the comprehensive enhancement of mechanical properties would be more appropriately attributed to the synergy of the dual-phase configuration rather than to a single factor. We hope these discussions help clarify our viewpoint.

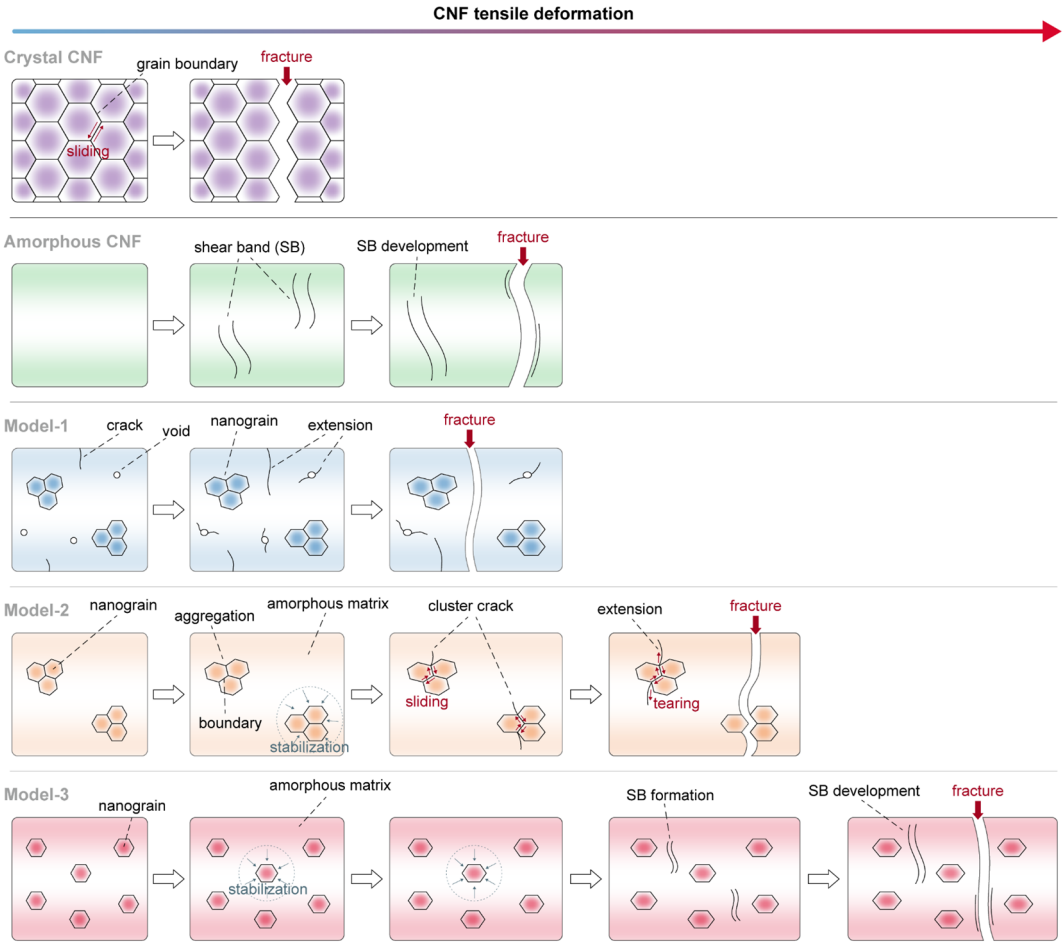

Revision Fig. 7. Analysis of the fracture mechanisms of CNFs with different crystal structures.

- **Revisions to *Paragraph 4 of Section 2.4* in the Manuscript**

On the other hand, the enhanced structural continuity of the disordered matrix, combined with the stabilizing effect of the nanocrystals, allows for improved stress transfer and dissipation, likely delaying the onset of shear band formation. These multiple deformation modes encourage the plasticity before the CNFs fracture.

<u>Minor Comment</u> #1:

In Fig.1b, it looks like the red arrows at the cracks, grain boundaries, and shear bands denote dislocation pile-ups. Could the authors use some other way to visualize such deformation mechanisms?

Response:

To make **Fig. 1b** clearer and more understandable, we have revised it with a new visualization that incorporates circles and labels to illustrate the deformation mechanism. We appreciate the reviewer for bringing this issue to our attention.

- **Revisions to *Fig. 1b* in the Manuscript**

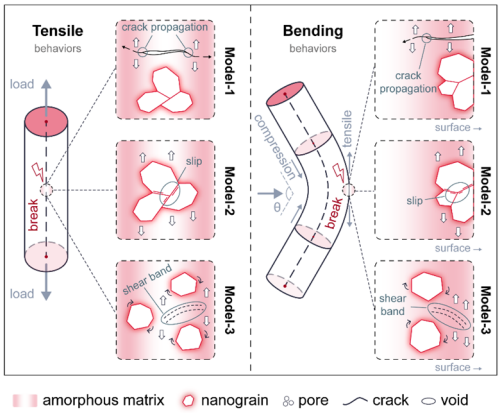

Fig. 1. (b) Stress analysis and fracture mechanisms of DP CNFs under tensile and bending loads.

Minor Comment #2:

The font size in Fig. 4i is too small. Can the authors use larger font size and an equal picture size for all other figures, including the supplementary ones. For example, supplementary Fig. 12 is not properly sized, compared to Fig. 12.

Response:

We thank the reviewer's suggestion and have carefully examined and revised all figures (including **Manuscript Fig. 4i** and the original **Supplementary Fig. 12**) in both the *Manuscript* and *Supplementary Information* to ensure consistent font sizes and plotting standards as much as possible.

- **Revisions to *Fig. 4i* in the Manuscript**

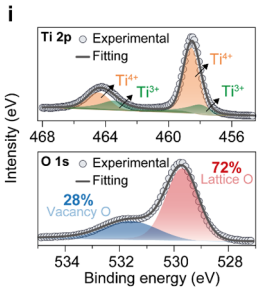

Fig. 4. (i) X-ray photoelectron spectroscopy analysis of the O 1s and Ti 2p spectra for the DP structure (Model-3).

- **Revisions to *Supplementary Information*** (original Fig. 12, now Fig. 11)

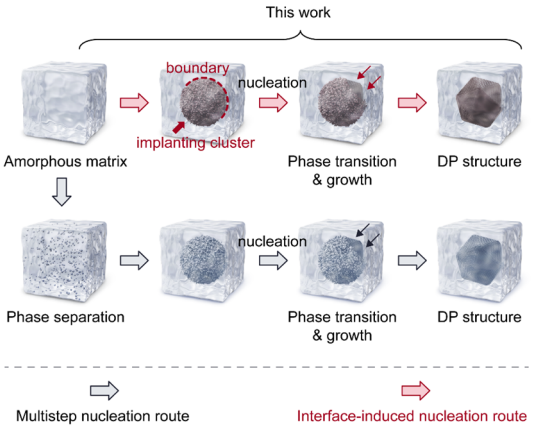

Supplementary Fig. 11. Schematic diagram of the nucleation-growth process. The nanograins within the disordered matrix follow the multistep nucleation route and the interface-induced nucleation route, respectively.

<u>Minor Comment</u> #3:

The authors demonstrate that nucleation regulation enhances strength and deformability. In Model-3, random nucleation points result in nanograins emerging further apart, preventing aggregation. However, how does the algorithm prevent interleaving where grains grow and coalesce together? Could the authors provide more details on this aspect?

Response:

We are encouraged by the reviewer's interest in nucleation regulation. As described in the manuscript, SP-sol and LP-sol were combined to prepare the binary sol, which was then electrospun into precursors with embedded nanoclusters. Such precursor nanofiber possessed a unique pre-configuration, consisting of a matrix formed by loosely stacked Ti–O chains and dense nanoclusters formed by cross-linked Ti–O networks.

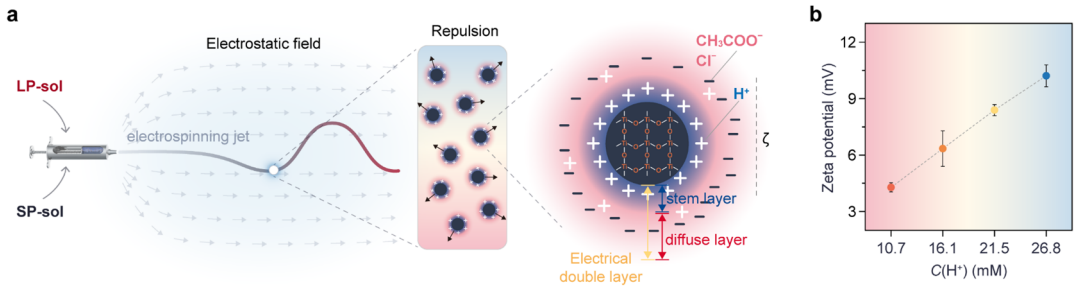

Revision Fig. 8. (a) Schematic diagram of the electrospinning process for binary sols and the electric double-layer structure of spherical particles. (b) Zeta potential analysis of sols with varying ionic concentrations.

The uniform embedding of nanoclusters in the precursor is a key prerequisite for inducing non-aggregated nanograin growth, which relies on the effective regulation of spherical particles (SPs) in binary sols. According to the electrical double-layer (EDL) theory, there is a multi-layer structure for SPs comprising the particle surface, the stern layer and the diffuse layer (**Revision Fig. 8a**). Manipulating the EDL and SP dispersion by varying ionic concentrations is a facile method. In this work, this was achieved by adjusting the amount of HCl. Increasing the EDL thickness would facilitate mutual repulsion and dispersion between suspended particles. As shown in **Revision Fig. 8b**, Zeta potential measurements confirm a positive correlation between ionic concentration and the stability and dispersion of sols. During electrospinning, the whipping motion of

the charged jet promotes the migration of SPs, with EDL repulsion playing a key role in preventing the final aggregation of nanoclusters. However, there is an upper limit to the HCl concentration, dictated by the quality of fiber formation, as excessively high conductivity could compromise nanofiber morphology or even prevent fiber formation. Thus, a rational increase in ionic concentration (as used in *Section 4.1*) would ensure the uniform dispersion of dense nanoclusters in the precursor, which is the key prerequisite for avoiding the aggregative growth of grains.

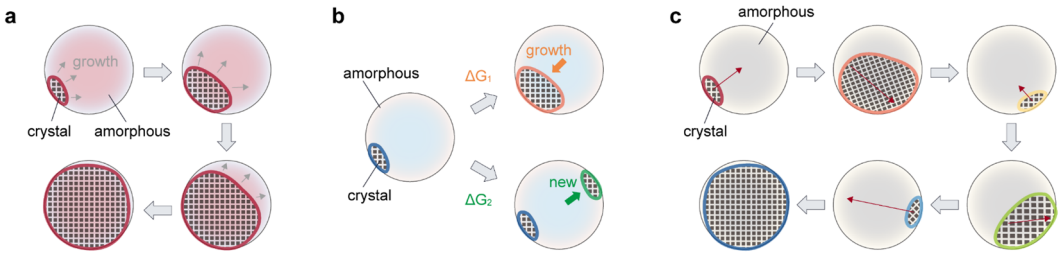

Revision Fig. 9. Analysis of crystallization-growth processes within dense nanoclusters.

On the other hand, the subsequent crystallization-growth behavior inside the dense nanocluster also need to be carefully analyzed. Firstly, it has been shown that the implantation of dense nanoclusters promotes crystallization, as evidenced by the decrease in activation energy (ΔG) for crystallization, as depicted in **Manuscript Fig. 3a**. Wang *et al.* (*J. Phys. Chem. C* **2020**, 124, 15533) observed that crystallization readily initiates at the boundaries of dense clusters and grows diffusively toward the clusters interiors (**Revision Fig. 9a**). Admittedly, when the first site undergoes atomic rearrangement and crystallizes, the second site may also appear within the same nanocluster (**Revision Fig. 9b**). Nevertheless, the ΔG for path 1 (growth) is generally considered lower than that for path 2 (nucleation) (*J. Non-Cryst. Solids* **1990**, 117, 230). This results in a higher probability for path 1 occurring, and the continued development of this path favors the formation of an individual crystal within the original cluster space. Furthermore, cutting-edge studies (*Science* **2021**, 371, 498) have reported “structural oscillations” during crystal formation (**Revision Fig. 9c**). Besides metal substrates, this phenomenon has also been observed in metal oxides (**Revision Fig. 10**, *Mater. Horiz.* **2022**, *9*, 1670). Dynamic reversible fluctuations between disordered and ordered states may also promote the unification, and thus independence of crystals within single clusters.

[figure redacted]

Revision Fig. 10. (a) In-situ observation of the formation of NiO nanocrystals, illustrating "structural oscillations" between the crystalline and amorphous states. (b) Time-labeled contour plots of crystalline boundaries. (c) Evolution of the crystalline fraction. Copyright 2022, The Royal Society of Chemistry (*Mater. Horiz.* **2022**, 9, 1670).

The phenomenon of nanograin aggregation in Model-2 may be attributed to the recently reported non-classical nucleation theory. The aggregation of clusters could occur during the phase separation and nucleation migration stages. However, by pre-implanting dense nanoclusters, this step was skipped during Model-3 incubation, transitioning directly to the classical nucleation theory stage (**Revision Fig. 11**). We expect that these analyses will contribute to a better understanding of the Model-3 formation. The relevant references have been added to the manuscript:

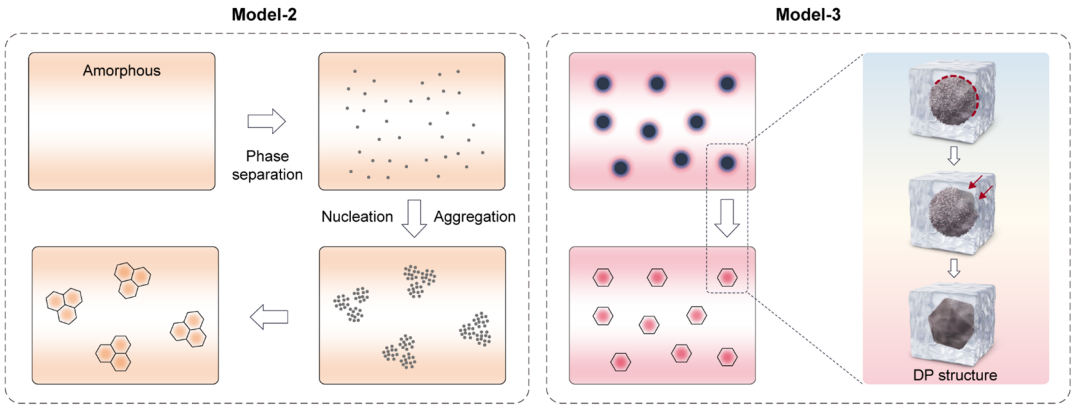

Revision Fig. 11. Comparison of the structure formation processes of Model-2 and Model-3.

- **Revisions to *References* in the Manuscript**

54. Jeon S, *et al.* Reversible disorder-order transitions in atomic crystal nucleation. *Science* **371**, 498 (2021).

55. Wang T, *et al.* In situ observation of nucleation and crystallization of a single nanoparticle in transparent media. *J. Phys. Chem. C.* **124**, 15533 (2020).

56. Zhang Z, *et al.* Multistep nucleation visualized during solid-state crystallization. *Mater. Horiz.* **9**, 1670 (2022).

<u>Minor Comment</u> #4:

The difference in the SAED patterns between Model-2 and Model-3, as shown in the insets of Fig. 3e, is not clearly visualized. Also, please state the purpose/significance of such patterns.

Response:

We would like to draw the reviewer's attention to the clearer SAED patterns of Model-2 and Model-3 shown below (**Revision Fig. 12**). As you mentioned, there is no obvious difference between their SAED patterns, as both exhibit amorphous halos coupled with anatase diffraction spots. This observation highlights that they possess similar crystalline/amorphous dual-phase features, except their different nanocrystal distribution. In the manuscript, the XRD patterns, BET specific surface areas, SAXS curves also emphasize this. This setup facilitates controlled experiments and enables the investigation of CNF mechanical behaviors with the dual-phase distribution as the sole variable.

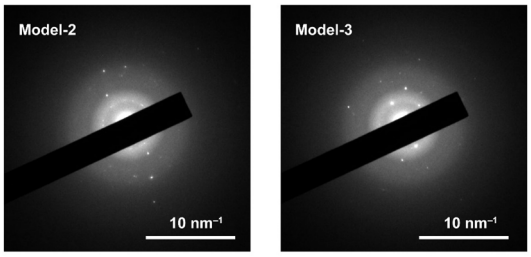

Revision Fig. 12. Comparison of SAED patterns of Model-2 and Model-3.

Minor Comment #5:

It is very interesting that controlled nucleation can result in a CNF with superior mechanical properties. While this finding can significantly improve the understanding of CNF's material response, it is worth exploring how a patterned nucleation scheme, as used in J. Appl. Phys. 134, 154301 (2023) and Appl. Phys. Lett. 122, 133101 (2023), where patterned nanodiamond regions are reported to be a better stress dissipator and conductor than random nucleation points, can influence the mechanical properties of Model-3?

Response:

We are very grateful to the reviewer for the insightful suggestions and inspiration. The reference you mentioned (*Appl. Phys. Lett.* **2023**, 122, 133101) highlights a promising direction for future investigations into the mechanical optimization of CNFs. In this work, Zhao *et al.* theoretically studied dual-phase AlN composites using MD simulations, focusing on their mechanics and structural evolutions. Two patterned distribution models (square and triangular) were examined and compared with the random distribution model. It was found that the triangular distribution model made the shear band transition zone more resistant to activation. Moreover, in the triangular-distribution model, immature shear bands were better confined due to the limited space available for migration and bypassing around the ordered nanograins. Consequently, the ultimate strength of the dual-phase samples was enhanced.

Based on these findings, it is reasonable to speculate that a patterned design of nanocrystals could positively influence the mechanical properties of dual-phase CNFs. However, the primary challenge lies in the current lack of suitable methods for experimentally achieving such ordered design in CNFs. We have provided an outlook on this topic in the revised "Discussion" section and added relevant references.

- **Revisions to *Discussion* in the Manuscript**

In the future, further efforts toward optimizing the mechanical properties of single CNFs are anticipated. One potential avenue is utilizing Model-3 as a platform to systematically modulate the size and quantity of nanograins (Supplementary Fig. 26), thereby gaining insights into how the volume fraction of the nanocrystal domain affects the evolution of the DP structure under loading. Accelerating this process could benefit from the incorporation of effective medium theories[70]. With appropriate modifications,

these classical theories are expected to simplify structure-mechanics relationships and offer predictive and guiding information. Another promising direction lies in the patterned design or orderly arrangement of nanocrystal regions within amorphous matrices. A more ordered and uniform distribution is predicted to suppress shear-band activation, and meanwhile constrain the migration and bypassing of disordered atomic clusters, thereby further promoting the mechanical strength and strain limits[27].

Reviewer #2:

I co-reviewed this manuscript with one of the reviewers who provided the listed reports. This is part of the Nature Communications initiative to facilitate training in peer review and to provide appropriate recognition for Early Career Researchers who co-review manuscripts.

Response:

We would like to thank the reviewer for the valuable feedback on our work. In response to the joint comments from you and Reviewer #1, we have optimized the MD simulations and refined the methodological details. Additionally, we have deepened our understanding of the mechanisms behind nucleation regulation and the mechanical enhancement of CNFs, providing relevant clarifications. From the perspectives of effective medium theories and nanocrystal patterned designs, we present an outlook on promising directions for further mechanical optimization of CNFs. Furthermore, we have improved the writing and visualization standards to ensure that the viewpoints presented are clear and convincing. We hope these revisions and clarifications will further enhance the quality and depth of the manuscript.

Reviewer #3:

The present manuscript by Qiang *et al.* reports on the synthesis and thorough structural and mechanical characterization of three distinct model TiO_2 ceramic nanofibers in the ~300 nm range. The authors show as stepwise improvement of mechanical characteristics of the individual fibres by (I) removal of multi-scale defects (model1 > model2) and (II) de-clustering of the nanocrystalline TiO_2 grains within the amorphous matrix (model2>model3). This structural optimization has been initially studied using MD simulations to guide the synthesis route. The authors have presented a ligand exchanged linear-particle sol, which was able to be electrospun without any polymer templates, reducing the formation of larger defects to a minimum. Furthermore, the addition of small percentages of spherical-particle sol was used to achieve well separated nucleation spots for nanocrystals, reducing the formation of stress-concentrating grain boundaries. The resulting improvement in mechanical response was investigated using state-of-the art nanomechanical testing for single fibres (PTP-tension) experiments as well as a creative, albeit not very accurate, way of estimating flexibility (in-situ fibre bending).

The authors have presented their train-of-thought and execution in an easy-to-follow and intuitive manner. The experimental investigations seem sound and the combination of different methods for structural (SEM, TEM, XRD) as well as energetic/chemical (DSC, DMA, XPS) investigations spark confidence in their conclusions. The work has been conducted on a well-studied model material system, but the results should be applicable for a wide variety of ceramics, potentially leading to novel designs in various 2D (fibre mats) or 3D (aerogels) applications.

A few minor questions that should be addressed:

Response:

We are very grateful to the reviewer for the meticulous review. These positive feedback has greatly encouraged us and contributed to enhancing the accuracy and reproducibility of this work. To address the reviewer's concerns regarding the in-situ mechanical tests, we conducted additional replications of the tensile and bending tests on single CNFs to confirm their mechanical behaviors. Furthermore, we thoroughly revised and refined the detailed descriptions of the in-situ mechanical experiments to elucidate the methodology for accurately obtaining stress-strain data. Finally, based on our understanding, we uncovered the mechanism underlying the differences in mechanical behaviors between Model-2 and Model-3. We hope these modifications and clarifications could meet the reviewer's requirements.

Comment #1:

While I understand that the chosen mechanical in-situ investigations are not trivial to perform, having only one experiment per material state does not spark a lot of confidence in the reproducibility of the results. Have the authors conducted multiple experiments? If so it would be beneficial to show the results at least as supplementary material to give the reader an idea about the uncertainties in yield onset and ductility values. The same is true for the fibre bending experiments.

Response:

We appreciate the reviewer's kind reminder. As you mentioned, in-situ mechanical experiments are indeed challenging to perform. Nevertheless, repeating these in-situ experiments is essential to ensure the reliability of the findings and conclusions.

To address this, we conducted additional in-situ tensile experiments on single CNFs, successfully reproducing the stress-strain curves of the experimental samples corresponding to the three models. The results show that the ultimate strength and strain limits of Model-1 are much lower than those of Model-2 and Model-3, consistent with the results presented in the manuscript. In addition, Model-3 still exhibits further improvements over Model-2 in key mechanical properties, including ultimate strength, strain limit, Young's modulus, and toughness. Furthermore, Model-3 demonstrates plasticity in the final stage of deformation. Specifically, it reaches the elastic strain limit initially due to the accumulation of recoverable interatomic bond elongation. After surpassing a strain threshold of ~4.65%, Model-3 begins to yield and undergo strain hardening. Eventually, Model-3 achieves an ultimate strength of ~1.02 GPa and a total strain of ~7.43%. In the original manuscript, Model-3 had an ultimate strength of ~1.04 GPa and a total strain of ~8.44%, comprising ~5.34% elastic strain and ~3.10% plastic strain. While minor deviations in absolute values may arise due to experimental errors and slight variations between sample batches, it is noteworthy that the replications results are highly consistent with the manuscript' conclusions. Both the mechanical behavior comparisons across models and the overall trends confirm the reproducibility and reliability of the findings.

We have added the relevant experimental data to *Supplementary Information* and revised the *Manuscript* accordingly. Additionally, we repeated the in-situ bending experiments as well, to further confirm the flexibility of CNFs.

- **Revisions to *Paragraph 3 of Section 2.4* in the Manuscript**

Also, these mechanical characteristics were further validated through repeated in-situ tests (Supplementary Fig. 22 and Fig. 23).

- **Revisions to *Supplementary Information***

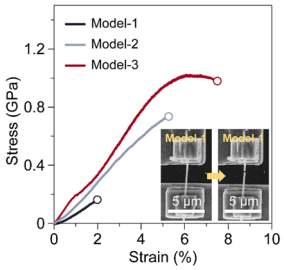

Supplementary Fig. 22. Stress-strain curves of experimental samples corresponding to the three models were successfully reproduced. While minor deviations in absolute values may result from experimental errors and slight variations between samples batches, it is noteworthy that the replications are highly consistent with the conclusions of the manuscript, both in terms of mechanical behaviors and overall trends.

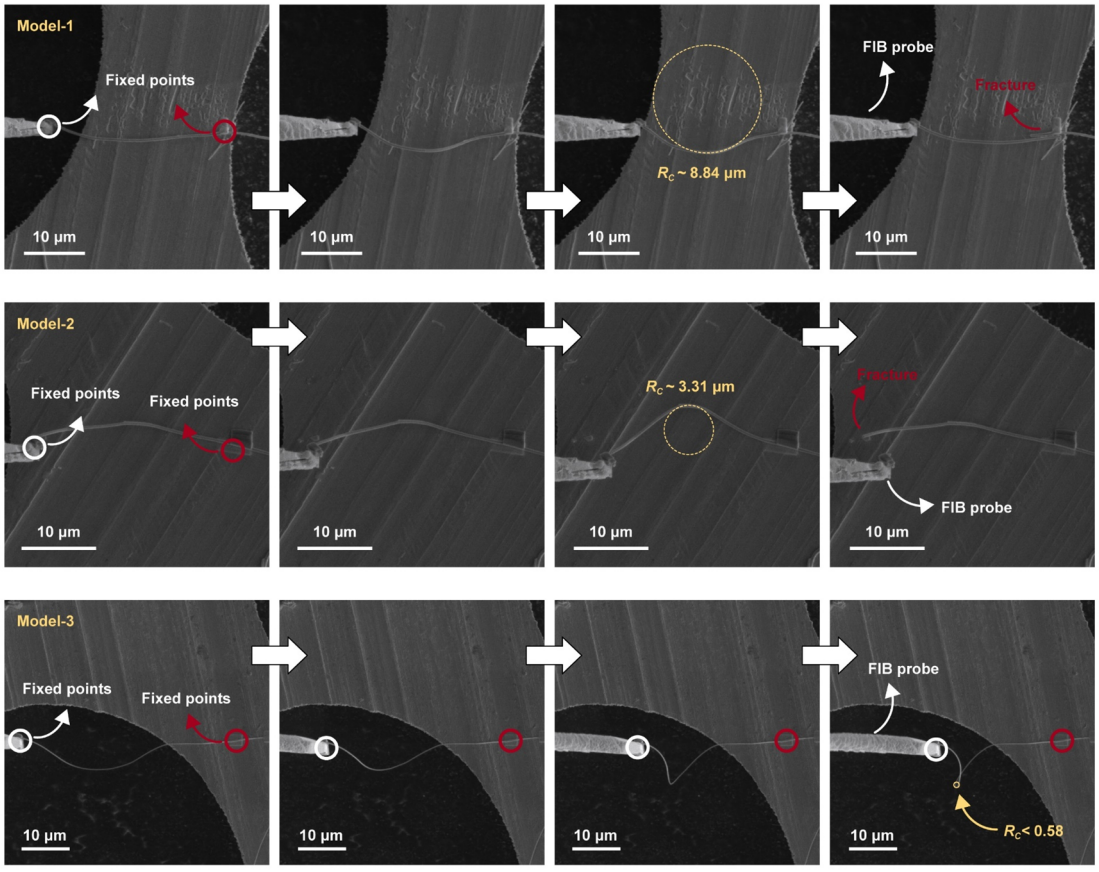

Supplementary Fig. 23. The flexible features of experimental samples corresponding to the three models were successfully reproduced.

Comment #2:

The authors never state how they obtain stress and strain measurements. Do they know the exact fibre diameter for the individual experiment or do they use an average of their previous measurements? Is strain measured from the in situ images? Are their initial fiber lengths always the same? Otherwise, strain-at-fracture cannot be a fair comparative measure for ductility. Why is the elastic modulus considerably different between the model2 and model3 case? Model1 makes sense, based on the defects (voids,cracks) and maybe some residual organic template content, but I'm puzzled by the difference between 2 and 3.

Response:

We thank the reviewer for providing us with the opportunity to clarify this issue. The tensile testing of single CNFs was performed using a combination of FIB techniques, PTP devices, nanoindentation instruments, and in-situ SEM. As the reviewer correctly pointed out, it is crucial to explain the quantification procedure for the stress-strain curve, which involves key parameters such as elongation, diameter, and cross-sectional area of the CNF. Hence, we provide a detailed discussion of this procedure below.

Specifically, the FIB technique was used to tailor single CNFs, which were then transferred and fixed onto the sample area of the PTP device. Next, SEM was employed to measure the initial length (L_0) and average diameter (d) of each CNF sample. The initial length (L_0) of each CNF was defined as the distance between two fixed points, and L_0 were controlled within a similar range for a fair comparison as much as possible (the distance of Model-1has been optimized in replication, **Supplementary Fig. 22**). The cross-sectional area of each CNF was calculated by approximating the nanofiber as a cylinder, using the formula $A=\pi d^2/4$. Before tensile testing, a conductive diamond planar punch with a diameter of 20 μm was calibrated and then used for tensile testing in displacement-controlled mode at a rate of 5 nm s^{-1} until the onset of fiber fracture. Force-displacement data were dynamically recorded (**Revision Fig. 13**), along with real-time video capture. The tensile increment (ΔL) and strain ($\Delta L/L_0\times100\%$) were measured based on in-situ SEM recordings. Since the force-displacement curves include contributions from both the PTP device and the CNF sample, quantifying the tensile mechanics requires subtracting the contribution of the PTP device. With the obtained cross-sectional area and strain limits, we accurately extracted the stress-strain

curves of the test samples. *Section 4.4* has been carefully revised to clarify this quantification procedure.

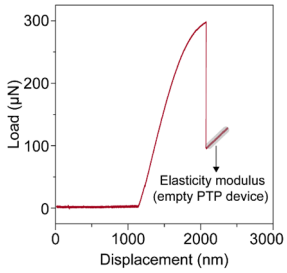

Revision Fig. 13. Representative load-displacement curve of CNFs (Model-3).

- **Revisions to *Section 4.4* in the Manuscript**

In-situ tensile tests were conducted using a Picoindenter 85 nanoindenter (Pi-85) integrated within a Quanta 250 FEG SEM, coupled with a PTP device. Individual CNFs were fixed onto the PTP sample area via FIB techniques[9, 29, 41]. Their average diameters and initial lengths were measured based on SEM observations. The cross-sectional area of each cylindrical CNF was calculated with its diameter, while the initial length was defined as the distance between two fixed points. These measurements were essential for the quantitative analysis of mechanical properties. Prior to testing, a conductive diamond flat punch with a diameter of 20 μm was calibrated. The flat probe was then positioned to contact the semi-circular end of the CNF mounted on the PTP device. Tensile testing was performed in displacement control mode at a rate of 5 nm s^{-1} until fracture occurred. Force and displacement data were dynamically recorded and and concurrently captured via real-time movie. The resulting force-displacement curve contained contributions from both the PTP device and the CNF sample. Thus, the inherent contribution of the PTP device was subtracted to determine the force applied to the CNF sample. Bending tests were carried out using a Thermo Scientific Helios 5 UX FIB-SEM.

Based on the single-nanofiber mechanical tests, Model-1 was found to be significantly weaker than Model-2 and Model-3, which is readily understood. This is primarily attributed to the structural defects in Model-1, such as pores, cracks, and voids, which act as the weakest links under tensile loading, leading to stress concentrations and crack propagation. In contrast, understanding the factors responsible for the mechanical variability between Model-2 and Model-3, particularly in terms of elastic

modulus, requires a more detailed analysis. We think that a careful comparison of the fracture mechanisms in different CNFs is necessary.

(i) Crystalline CNFs typically exhibit a polycrystalline structure with numerous grain boundaries. During tensile deformation, these grain boundaries are prone to slipping and tearing, leading to the formation and rapid propagation of cracks, and ultimately brittle fracture (**Revision Fig. 7**).

(ii) Amorphization has overcame this issue to some extent in CNFs due to the absence of obvious grain boundaries. The fracture of amorphous ceramics is generally initiated by the activation and development of shear bands. However, the simplistic and homogeneous structure of amorphous CNFs results in random and unconstrained initiation of shear bands, which limits further mechanical enhancement.

(iii) In this regard, the dual-phase structures of Model-2 and Model-3, consisting of nanograins embedded within an amorphous matrix, offer significant advantages. The embedded nanocrystal regions help stabilize the surrounding disordered atomic clusters (*Ceram. Int.* **2019**, 45, 19845; *Nature* **2022**, 606, 909; *Nat. Mater.* **2023**, 22, 42), thereby dissipating stress and delaying the activation of shear bands. However, once a certain strain threshold is reached, the boundaries within the nanograin clusters of Model-2 are likely to experience stress concentration, leading to grain boundary slip and tearing, which results in crack propagation and fracture. In contrast, the uniformly distributed nanocrystal regions of Model-3 could fully exploit the dual-phase configuration to promote multiple deformation mechanisms (*Int. J. Plast.* **2020**, 134, 102837), such as bond switching (*Nat. Commun.* **2010**, 1, 24; *Nano Lett.* **2016**, 16, 105; *Science* **2019**, 366, 864; *Science* **2022**, 378, 371) and grain rotation (*Science* **2024**, 386, 49). These rendered the sufficient stress dissipation and the delayed activation of shear bands, allowing Model-3 to achieve higher tensile strain thresholds.

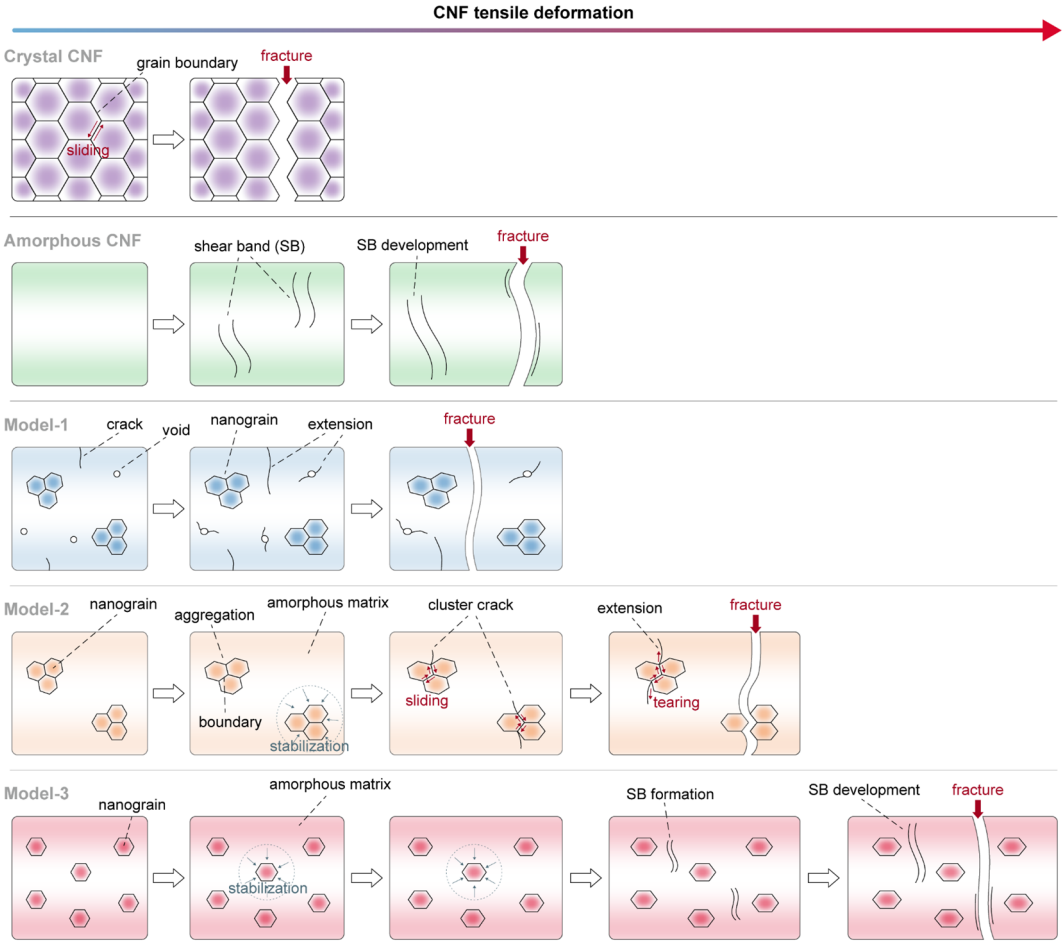

Revision Fig. 7. Analysis of the fracture mechanisms of CNFs with different crystal structures.

Furthermore, as discussed regarding the mechanism of "nanocrystal regions stabilizing the surrounding disordered atomic clusters", the more dispersed distribution of nanocrystals in Model-3 may further enhances this effect. For example, Zhao *et al.* (*Ceram. Int.* **2019**, 45, 19845) reported that the nanocrystal distribution markedly influenced both the structural evolution under tensile loading and the final mechanical behavior for dual-phase AlN. They found that patterned designs led to a more ordered and uniform distribution of nanograins, making the shear-band transition zone difficult to activate. Additionally, sufficiently dispersed nanograins spare less space available for the migration and bypassing of disordered atomic clusters and immature shear bands, which improves the material's ability to resist deformation. Therefore, we conclude that Model-3 has an optimized dual-phase interface compared to Model-2, featuring a larger internal interfacial surface area and a more extensive "stabilized" region (**Revision Fig. 14**). These factors collectively contribute to the higher ultimate strength and Young's

modulus observed in Model-3. We hope these analyses and explanations help clarify the differences in mechanical properties among the models.

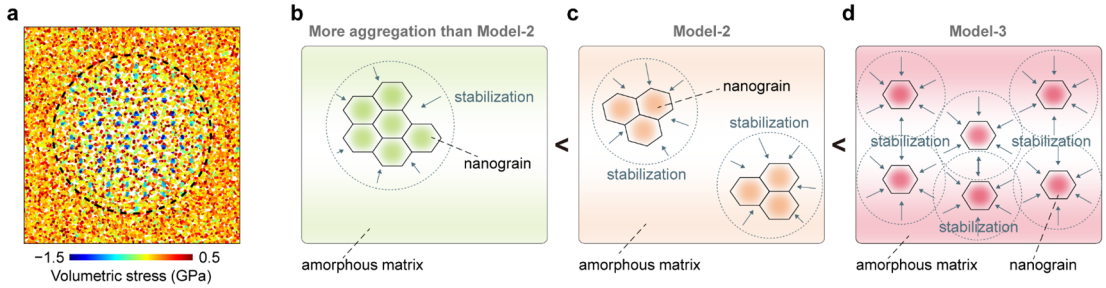

Revision Fig. 14. (a) MD stress field of a nanocrystal region and its surroundings within the dual-phase structure (Model-3). (b-d) A more dispersed and uniform distribution of nanocrystal regions enhances their "stabilization" effect on the surrounding disordered atomic clusters.

Reviewer #4:

In this study, the authors demonstrate a crystalline/amorphous dual-phase TiO2 nanofiber that combines high strength, good flexibility, and room-temperature plasticity through an internal-interface regulation strategy. It is based on an innovative method for synthesizing ceramic nanofibers, which allows for impressive control over the growth and evolution of nanocrystals. Given the inherent brittleness and limited deformability of ceramic materials, such comprehensive optimization of their mechanical properties is both urgent and valuable, making this finding attractive. However, several aspects require further revision and clarification, such as how the micromechanical optimization of individual nanofibers influences the macroscopic properties. Overall, this work is interesting and possessing novelty, with well-structured content and coherent logic. I believe that, following the necessary revisions, this manuscript is worthy of consideration for publication in Nature Communications.

Response:

We are grateful to the reviewer for these important comments, which have significantly enhanced the completeness and logical flow of the manuscript. In response to the reviewer's concerns, we focused on analyzing the impact of the mechanical integration of single CNFs on the macroscopic properties of their derived aggregates. Additionally, we provided an in-depth discussion on the feasibility of defect engineering for enhancing CNFs. Furthermore, we emphasized the structure and rheology of SP-sol and LP-sol, as these aspects are crucial for understanding the feasibility of direct spinnability and nucleation regulation. Lastly, we have supplemented the data as comprehensively as possible, including but not limited to the phase structure evolution of Model-2 and real-time movies of the in-situ mechanical tests. We hope these modifications and clarifications could meet the reviewer's expectations.

Comment #1:

In the introduction, the authors discuss the potential for achieving plasticity in ceramics through the deliberate creation of crystal defects and cite related studies. However, they also claim that this approach may not be applicable to ceramic nanofibers (Lines 79-82). What is the basis for this assertion?

Response:

We thank the reviewer for providing us with the opportunity to clarify this issue. Admittedly, the compressive plasticity of ceramic materials has been reported to be enhanced through the deliberate manipulation of crystal defects, as demonstrated in the studies by Shen and Li *et al.* (*Sci. Adv.* **2019**, *5*, eaaw5519; *Sci. Adv.* **2024**, *10*, eadj4079). Techniques such as flash sintering or high-temperature pretreatment have been employed in defect engineering of ceramic oxides to achieve the substantial introduction of crystal defects. Under compressive loading, room-temperature plasticity is achieved through mechanisms like grain boundary sliding or dislocation stacking. However, compared to compressive deformation, achieving tensile plasticity is significantly more challenging because the inherent defects in ceramic materials tend to expand under tensile loading, often resulting in catastrophic fracture.

Cutting-edge studies have led us to reconsider this perspective, which has realized the tensile plasticity in ceramic materials through metal-induced interfacial defects (*Science* **2024**, *385*, 422). However, it is important to note that such defect engineering not only fails to strengthen the ceramic material but instead weakens its ultimate strength, as reported. Therefore, the defect engineering may still be considered inapplicable to CNFs, as it has the potential to provide plastic deformation but may also weaken tensile strength. This would contradict the goal of achieving a comprehensive optimization of the mechanical properties of CNFs. As discussed in the manuscript, the mechanical properties of individual CNFs fundamentally determine the macroscopic performance of the monolithic material. Any deficiencies in the integration of mechanical properties (such as strength, tensile strain, or flexibility) could result in catastrophic structural failure of the monolithic material under complex stress environments.

We hope these analyses and discussions help clarify the key viewpoints. Furthermore, to enhance coherence, we decided to merge the *Paragraph 3* and *4* of the "*Introduction*" section into a single paragraph.

Comment #2:

The development of a directly spinnable sol appears to be critical for achieving a dense structure in ceramic nanofibers. The manuscript notes that traditional methods for synthesizing ceramic nanofibers rely on polymer templates. Why does the LP-sol synthesize in this study exhibit spinnability? What is the origin for its spinnability? This point needs to be clarified.

Response:

We are encouraged by the reviewer's interest in this issue, which lies at the core of the innovative approach central to this study. Conventional methods for synthesizing CNFs typically rely on polymer templates. In contrast, the LP-Sol developed in this study exhibits direct spinnability, which we attribute to its unique shape and structure. Generally, the synthesis of sols using metal alkoxides as monomers is unconstrained, leading to rapid polymerization and the formation of branching structures prone to irreversible 3D networks. However, we have successfully manipulated the hydrolysis-condensation process through coordination modification. By combining an elaborate synthesis process with rational molar ratios, we enabled the polycondensation reaction of the monomers to proceed in an approximately linear mode, as evidenced by the evolution of sol-gel rheology (**Manuscript Fig. 2c** and **2d**).

The rheology of LP-sol satisfies the Huggins equation, distinguishing it from SP-sol, which contains spherical particles as dispersions. The behavior of LP-sol is more akin to that of organic polymer solutions (**Revision Fig. 15a**). The entanglement and interactions between the chain-like particles in LP-sol can be readily associated with the spinning process, which is critical to its functionality, much like the spinning mechanism of organic polymer solutions (**Revision Fig. 15b**).

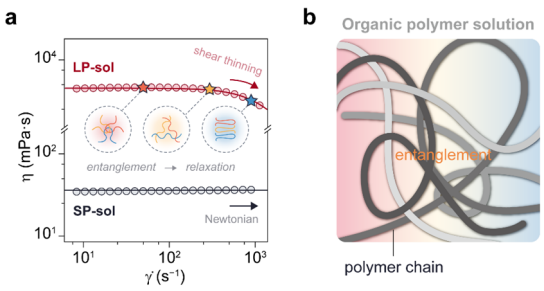

Revision Fig. 15. (a) Plots of η versus the shear rate of SP-sol and LP-sol (α = 0.8). Inset: entanglement-relaxation behaviors of linear particles. (b) Schematic diagram illustrating the entanglement of polymer chains, critical for the spinning properties.

Comment #3:

For this work, the dual-phase configuration is essential for achieving the desired final structure. If the SP-sol were to aggregate, controlling the growth of nanocrystals would be highly challenging. In other words, how to ensure that SP-sol does not aggregate?

Response:

The reviewer has pointed out the key factor in Model-3 formation. The uniform embedding of nanoclusters in the precursor is crucial for achieving the final structure of Model-3, which requires the effective regulation of spherical particles (SPs) in binary sols. According to the electrical double-layer (EDL) theory, there is a multi-layer structure for SPs comprising the particle surface, the stern layer and the diffuse layer (**Revision Fig. 8a**). Manipulating the EDL structure and the consequent dispersion of SPs by adjusting the ionic concentration is a straightforward method. In this study, it was achieved by varying the HCl amount. Typically, increasing the EDL thickness would facilitate the mutual repulsion and dispersion between suspended particles. As shown in **Revision Fig. 8b**, Zeta potential measurements confirm a positive correlation between ionic concentration and the stability and dispersion of sols. During electrospinning, the whipping of the charged jet promotes the migration of SPs, with the EDL repulsion playing a key role in preventing the final aggregation of nanoclusters. However, there is an upper limit to the HCl amount, which is constrained by the fiber-forming quality, since excessively high conductivity would compromise nanofiber morphology or even prevent nanofiber formation. Thus, a rational increase of the ionic concentration (*Section 4.1*) would ensure the uniform dispersion of dense nanoclusters in the precursor, which is essential for avoiding the aggregative growth of grains.

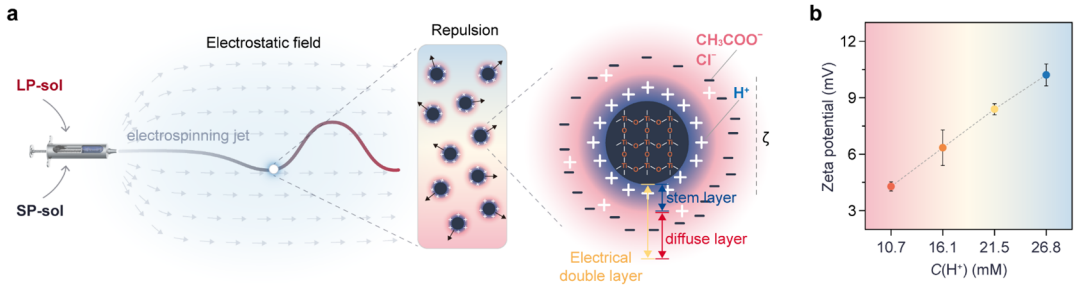

Revision Fig. 8. (a) Schematic diagram of the electrospinning process for binary sols and the electric double-layer structure of spherical particles. (b) Zeta potential analysis of sols with varying ionic concentrations.

<u>Comment</u> #4:

It is recommended to compare the crystallization behavior of Model-2 and Model-3 using XRD analysis. Additionally, Fig 2i does not indicate the sintering temperatures corresponding to the different curves.

Response:

We thank the reviewer for the important suggestion, and we have revised **Fig. 2i** accordingly. Meanwhile, we have included the XRD analysis of Model-2 to further elucidate its phase structure evolution.

- **Revisions to *Paragraph 3 of Section 2.2* in the Manuscript**

X-ray diffraction (XRD) patterns display the phase structure evolution of the binary pre-configuration (Fig. 2i) compared to its counterparts without embedded nanoclusters (Supplementary Fig. 12).

- **Revisions to *Supplementary Information***

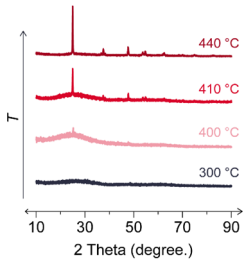

Supplementary Fig. 12. XRD patterns of phase structure evolution of the precursor for Model-2.

Comment #5:

In Section 2.4, I noticed that the authors provided videos for the in-situ tensile test of Model-1 and the in-situ bending test of Model-3. Please include additional videos that cover the in-situ tensile and bending tests for all models, to improve the completeness of the manuscript.

Response:

We are very grateful to the reviewers for their reminders. Movies of in-situ tensile tests and bending tests of all models have been added.

- **Revisions to *Supplementary Information***

Supplementary Movie 1.

The corresponding real-time movie was dynamically recorded during the tensile tests (Model-1)

Supplementary Movie 2.

The corresponding real-time movie was dynamically recorded during the tensile tests (Model-2)

Supplementary Movie 3.

The corresponding real-time movie was dynamically recorded during the tensile tests (Model-3)

Supplementary Movie 4.

The corresponding real-time movie was dynamically recorded during the bending tests (Model-1)

Supplementary Movie 5.

The corresponding real-time movie was dynamically recorded during the bending tests (Model-2)

Supplementary Movie 6.

The corresponding real-time movie was dynamically recorded during the bending tests (Model-3)

Comment #6:

The authors emphasize the significance of enhancing the mechanical properties of individual fibers, noting that these properties determine the macroscopic mechanics of the nanofiber aggregate. However, the manuscript provides only limited demonstrations of this. I suggest further exploring the mechanical impact of single nanofibers on the aggregates they form to offer readers a more comprehensive understanding.

Response:

We thank the reviewer for raising this critical concern. As emphasized in the manuscript, the comprehensive mechanical properties of single ceramic nanofibers are fundamental to ensuring the viability and industrialization of the macroscopic materials derived from them. From a deeper perspective, tensile strength, axial strain limit, and flexibility are likely the most important mechanical properties of single CNFs. These properties collectively influence the ability of these structural units to absorb energy and transfer loads, ultimately determining the macroscopic material's capacity to effectively avoid stress concentrations and maintain structural stability. Similar to the concept of the barrel effect, a deficiency in any one of these mechanical properties can result in catastrophic structural failure of the overall material under complex stress environments.

Therefore, we assembled the synthesized Model-1, Model-2, and Model-3 into fibrous aerogels, labeled as MA-1, MA-2, and MA-3, respectively, to perform mechanical tests and comparisons aimed at revealing the correlation between the properties of single CNFs and the mechanical properties of their 3D aggregates. It is important to emphasize that the preparation process for these aerogel samples was identical, except for the use of different fibers as the building blocks, to ensure a fair comparison.

Compared to MA-1, MA-2 and MA-3 exhibited robust mechanical properties and could withstand large compressive loads, enduring compressive strains (ε) as high as 80% (**Supplementary Fig. 25**). In contrast, MA-1 cracked and collapsed after experiencing a compressive ε of only ~20%. The mechanical differences between the aggregates and the single CNFs showed high consistency. When comparing MA-2 and MA-3, it was observed that MA-3 demonstrated superior elasticity and strength at the same strain, particularly at ε ~80%, where its strength reached as high as ~20.4 kPa. This suggests that the 3D aggregates composed of Model-3 outperform those composed

of Model-2 in both Young's modulus and maximum strength. Specifically, MA-3 exhibits a linear elastic regime at $\varepsilon < 40\%$, a transition stage at $40\% < \varepsilon < 60\%$, and a densification regime at $\varepsilon > 60\%$. The dynamic mechanical properties of the aerogel samples were further analyzed using DMA. Notably, MA-3 exhibited consistent storage and loss moduli over three orders of magnitude in angular frequency. Moreover, its damping ratio remained more stable than those of MA-1 and MA-2 at high frequencies. In contrast, both the loss modulus and damping ratio of MA-1 fluctuated considerably at high frequencies. These findings highlight the importance of the excellent mechanical properties of individual CNFs in maintaining the structural stability of the aggregate materials derived from them.

We would like to draw the reviewer's attention to the fact that the former "Conclusions" section has been replaced with a new "Discussion" section. We have organized the findings mentioned above into the "Discussion" and added relevant fabrication process, description, and details to the supplementary information.

- **Revisions to *Discussion* in the Manuscript**

For applications with extreme mechanical environments, ceramic components are required to exhibit high strength, flexibility, and even plastic deformation. We have proved that the template-free synthesis method, combined with an interface-induced nucleation strategy, offer a promising solution to meet these demands. From a macroscopic perspective, we investigated how the mechanical integrations of single CNFs, including tensile strength, axial strain limit, and flexibility, affect the performances of the aggregates derived from them. For instance, the strategic assembly of CNFs into 3D aerogels revealed that those composed of synthesized Model-3 exhibit superior elasticity and structural stability compared to those of Model-1 and Model-2 (Supplementary Fig. 25). Notably, single-fiber defects are also fatal to the macroscopic mechanics, as evidenced by the collapse of the aerogel with Model-1 as the structural unit after only compressive ε ~20%, compared to the ε ~80% that Model-3 can robustly withstand. Observations of the macroscopic behavior of aggregates underscore the importance of improving the comprehensive mechanics of single CNFs, since which collectively determine their ability to absorb energy and transfer loads as structural units. In the future, further efforts toward optimizing the mechanical properties of single CNFs are anticipated. One potential avenue is utilizing Model-3 as a platform to systematically modulate the size and quantity of nanograins (Supplementary Fig. 26),

thereby gaining insights into how the volume fraction of the nanocrystal domain affects the evolution of the DP structure under loading. Accelerating this process could benefit from the incorporation of effective medium theories[70]. With appropriate modifications, these classical theories are expected to simplify structure-mechanics relationships and offer predictive and guiding information. Another promising direction lies in the patterned design or orderly arrangement of nanocrystal regions within amorphous matrices. A more ordered and uniform distribution is predicted to suppress shear-band activation, and meanwhile constrain the migration and bypassing of disordered atomic clusters, thereby further promoting the mechanical strength and strain limits[27].

- **Revisions to *Supplementary Information***

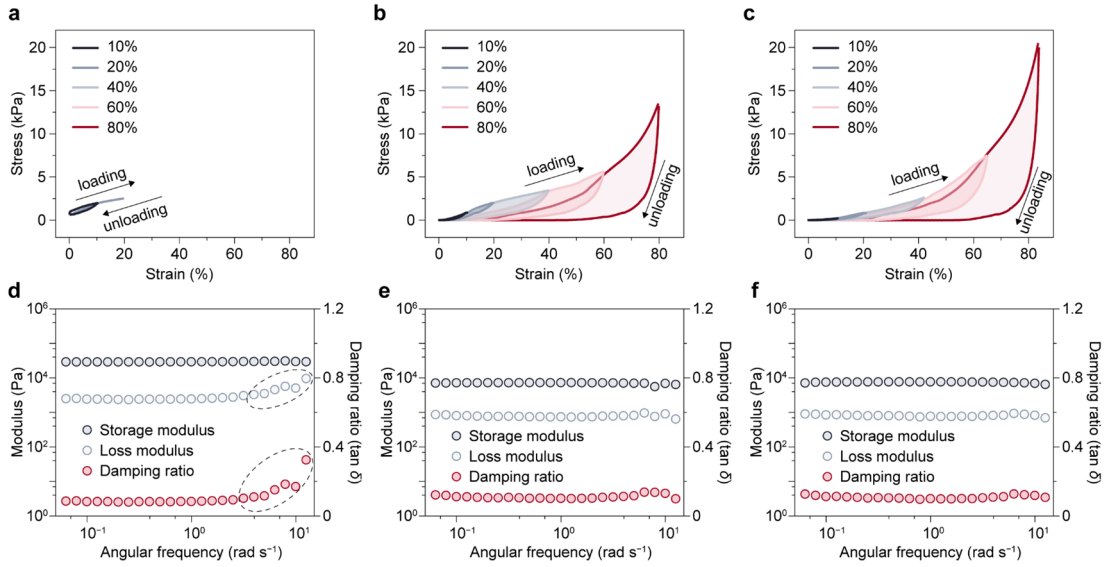

Supplementary Fig. 25. The synthesized Model-1, Model-2, and Model-3 were assembled into fibrous aerogels, and the dynamic mechanical properties of these 3D aggregates were analyzed and compared. (a-c) Curves showing the strength as a function of compressive strain for the aerogel samples composed of Model-1, Model-2, and Model-3, respectively, accompanied by a gradual increase in maximum strain during the cyclic loading and unloading process. (d-f) Frequency dependence of the storage modulus, loss modulus, and damping ratio of the aerogel samples consisting of Model-1, Model-2, and Model-3, respectively, under an oscillatory strain of 3%.

Comment #7:

What is the bulk density of the aerogels shown in Fig 4m? What preparation method and raw materials were used? Were any additional components introduced? How does the mechanical performance compare to aerogels prepared from Model-1 and Model-2?

Response:

We thank the reviewer for the attention to these details. The aerogel shown in Fig. 4m was composed of Model-3, with a bulk density of 5 mg cm^{-3}. To enhance the completeness of the manuscript, we have added details of the fibrous aerogel preparation process to the description in **Supplementary Fig. 25**. As mentioned in the response to comment #6, the mechanical properties of aerogels assembled from Model-3 are superior to those of Model-2 and Model-1. This underscores the importance of the excellent mechanical properties of individual CNFs in maintaining the structural stability of the aggregate materials derived from them.

- **Revisions to *Supplementary Information***

Supplementary Fig. 25. The synthesized Model-1, Model-2, and Model-3 were assembled into fibrous aerogels, and the dynamic mechanical properties of these 3D aggregates were analyzed and compared. (a-c) Curves showing the strength as a function of compressive strain for the aerogel samples composed of Model-1, Model-2, and Model-3, respectively, accompanied by a gradual increase in maximum strain during the cyclic loading and unloading process. (d-f) Frequency dependence of the storage modulus, loss modulus, and damping ratio of the aerogel samples consisting of Model-1, Model-2, and Model-3, respectively, under an oscillatory strain of 3%.

The preparation of these fibrous aerogels was accomplished using the freeze-template method[25]. First, the CNFs were dispersed in an aqueous solution and further processed using a high-pressure homogenizer. Subsequently, prepared silica sol binders were added to the dispersion and thoroughly stirred to ensure homogeneity. The silica sol binders were formulated with a molar ratio of tetraethyl silicate: ethanol: water: phosphoric acid at 1 : 45 : 46 : 0.002. The homogenized nanofiber dispersions were then frozen and freeze-dried for 24 h. Finally, the 3D aggregates were sintered at a temperature below the formation temperature of the hypocrystalline structure (~380 °C).

Comment #8:

Compared to Model-3 (Lines 424-426), what is the electronic structure of Model-2? Does Model-2 also exhibit oxygen vacancies? Please provide this information. Could these differences be the key factor behind their plastic properties?

Response:

We think the perspective suggested by the reviewers is critical. Comparing the electronic structures of Model-2 and Model-3 provides valuable insight into the differences in their mechanical properties (**Manuscript Fig. 4i**). Therefore, we have included the XPS spectra of Model-2, covering both O 1s and Ti 2p spectra (**Supplementary Fig. 24**). It is observed that the ratio of the integral area of vacancy O for Model-2 and Model-3 is very similar, at approximately 29% and 28%, respectively, indicating that their oxygen vacancy concentrations are also comparable. This suggests that oxygen vacancy concentration is not directly responsible for the differences in plasticity between the two models.

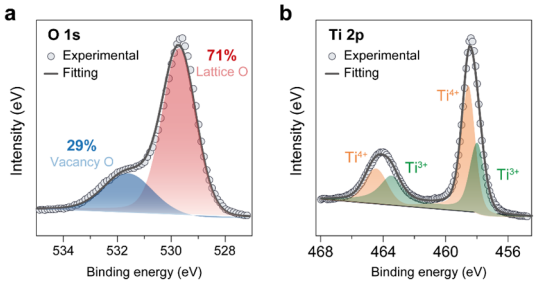

Supplementary Fig. 24. X-ray photoelectron spectroscopy for O 1s and Ti 2p spectra of dual-phase structure (Model-2).

Nevertheless, we believe that the presence of oxygen vacancies and the corresponding dangling bonds contributes to ceramic plastic deformation by enabling multiple deformation mechanisms, including bond-switching events. Frankberg *et al.* (*Science* **2019**, 366, 864) reported the plastic deformation behavior of metal oxides initiated by bond-switching. Their study demonstrates that the deformation of materials under shear and tensile loading becomes more diverse due to bond switching and rotation. They concluded that the plasticity observed in Al_2O_3 likely depends on the accumulation of bond-switching in localized atom groups. During deformation, the central Al atom can move into an adjacent space, forming a new bond with an O atom to replace the original bond. Furthermore, such bond-switching events have also been

observed in other studies on the plastic behavior of amorphous or dual-phase ceramic materials (*Nano Lett.* **2016**, 16, 105; *Science* **2022**, 378, 371).

On the other hand, in terms of promoting bond-switching events by vacancies and dangling bonds, Zhang *et al.* (*Nat. Commun.* **2010**, 1, 24) reported a strategy involving the induction of numerous oxygen vacancies and dangling bonds via high-energy electron beam treatment to improve the ductility of oxide ceramics. During deformation, these dangling bonds recombine with neighboring atoms, accompanied by the rotation and migration of associated atomic groups. Such artificially induced dangling bonds and vacancies are recognized to help overcome energy barriers and facilitate the initiation of bond switching. The repetition and accumulation of these bond-switching events ultimately support the plastic flow of the material. As shown in **Revision Fig. 5**, a broken bond creates a dangling silicon bond and a non-bridging oxygen atom. The non-bridging oxygen bonds with a different silicon atom, simultaneously causing this silicon to sever its bond with another oxygen. Consequently, the SiO_4 unit clusters undergo rotation and relocation.

[figure redacted]

Revision Fig. 5. The representative bond-switching event in SiO_2. Copyright 2010, Springer Nature. (*Nat. Commun.* 2010, 1, 24)

In view of these insights, it is reasonable to speculate in the original manuscript that some degree of bond-switching events could occur during the deformation of CNF, aligning with findings from studies on amorphous metal oxides. The intrinsic oxygen vacancies in Model-3, as evidenced by XPS, along with consequently dangling bonds, would play an essential role in facilitating these bond-switching events (as the absence of adjacent O atoms could make the central Ti atoms more susceptible to movement). The accumulation of such bond-switching events is one of the key factors that enables the deformations in the CNFs.

Response to Reviewers

We sincerely appreciate the reviewers for their constructive feedback.

Reviewer #1:

Response: We sincerely thank the reviewer for the comprehensive and meticulous review, helping us improve this study, especially the molecular dynamics sections.

Reviewer #2:

Response: We sincerely thank the reviewer for your suggestions and comments.

Reviewer #3:

Response: We sincerely thank the reviewer for the comprehensive and meticulous review, helping us improve this study, especially the single-nanofiber mechanic tests.

Reviewer #4:

Response: We sincerely thank the reviewer for the comprehensive and meticulous review, helping us improve this study, especially the nanofiber aggregate sections.